PHYSICAL REVIEW D **75,** 014506 (2007)

Quarkonium correlators and spectral functions at zero and finite temperature

A. Jakovác[*]
Institute of Physics, BME Budapest, Budafoki út 8, H-1111 Budapest, Hungary

P. Petreczky[†]
Physics Department, Brookhaven National Laboratory, Upton New York 11973, USA

K. Petrov[‡]
Niels Bohr Institute, Blegdamsvej 17, 2100 Copenhagen O, Denmark

A. Velytsky[§]
Department of Physics and Astronomy, UCLA, Los Angeles, California 90095-1547, USA
(Received 15 November 2006; published 19 January 2007)

We study quarkonium correlators and spectral functions at zero and finite temperature using the anisotropic Fermilab lattice formulation with anisotropy $\xi = 2$ and 4. To control cut-off effects we use several different lattice spacings. The spectral functions were extracted from lattice correlators with maximum entropy method based on a new algorithm. We find evidence for the survival of $1S$ quarkonium states in the deconfined medium till relatively high temperatures as well as for dissolution of $1P$ quarkonium states right above the deconfinement temperature.

DOI: 10.1103/PhysRevD.75.014506 PACS numbers: 11.15.Ha, 12.38.Aw

I. INTRODUCTION

The study of heavy quarkonium correlators at zero and finite temperature is interesting for several reasons. First, quarkonia are hadrons whose properties and structures are best understood; to the first approximation their properties can be described in terms of nonrelativistic potential. Also due to their small sizes they can provide a bridge between perturbative and nonperturbative QCD. On general grounds it is expected that quarkonia will melt at temperatures somewhat higher than the deconfinement temperature as a result of modification of interquark forces (color screening). Thus their properties at finite temperature can serve as an indicator of in-medium modification of interquark forces and help to understand the phenomenon of non-Abelian Debye screening in quark gluon plasma. Furthermore, it was suggested by Matsui and Satz [1] that color screening at high temperature will lead to quarkonium suppression which can serve as a signal of quark gluon plasma formation in heavy ion collisions. Quarkonium properties at finite temperature have been extensively studied in potential models [1–14]. However, the validity of potential models at finite temperature is doubtful. It is more appropriate to study modifications of quarkonium properties at finite temperature in terms of spectral functions. First principle calculations of the quarkonium spectral functions at finite temperature have become available only recently [15–17]. In the calculations of charmonium spectral functions which have been performed so far, the systematic errors were not well controlled. Although some features of the spectral functions extracted so far have been assigned to be due to lattice discretization effects, it has not been examined in detail which features of the charmonium spectral functions are physical and which are merely artifacts of the finite lattice spacing and analysis methods.

The aim of the present paper is twofold. First, we would like to study the properties of the quarkonium spectral functions in a large range of lattice spacings to control systematic effects both due to finite lattice spacing and limited number of data points. Second, we want to study quarkonium correlators at nonzero temperature to see what happens to different charmonium states above deconfinement. Having at hand results from different lattice spacings allows to check the cut-off dependence of these results. In addition to charmonium correlators we also calculate bottomonium correlators and spectral functions. Some preliminary results of this study have been presented in [18–21].

The rest of the paper is organized as follows. In Sec. II we discuss general properties of quarkonium correlators at finite temperature. In Sec. III we describe the analysis tools for the reconstruction of the quarkonium spectral functions. In Sec. IV we discuss our lattice setup used in the calculation of the charmonium correlators. In Sec. V we discuss charmonium spectral functions at zero temperature, emphasizing the systematic uncertainties of the analysis. Section VI deals with the temperature dependence of charmonium correlators. In Sec. VII we discuss the problem of reconstruction of charmonium spectral functions at finite temperature. Section VIII contains some results on

[*]Electronic address: jakovac@cern.ch
[†]Electronic address: petreczk@quark.phy.bnl.gov
[‡]Electronic address: kpetrov@nbi.dk
[§]Electronic address: vel@ucla.edu

charmonium correlators at nonzero spatial momenta. In Sec. IX and X we discuss our results for bottomonium correlators and spectral functions. Finally Sec. XI contains our conclusions. The reader not interested in technical details may skip Secs. II, III, and IV.

II. MESON CORRELATORS AND SPECTRAL FUNCTIONS

In this section we discuss the relation between the Euclidean meson correlators and spectral functions at finite temperature. It is straightforward to take the zero temperature limit.

Most dynamic properties of the finite temperature system are incorporated in the spectral function. The spectral function $\sigma_H(p_0, \vec{p})$ for a given mesonic channel H in a system at temperature T can be defined through the Fourier transform of the real time two point functions $D^>$ and $D^<$ or equivalently as the imaginary part of the Fourier transformed retarded correlation function [22],

$$\begin{aligned}\sigma_H(p_0, \vec{p}) &= \frac{1}{2\pi}(D_H^>(p_0, \vec{p}) - D_H^<(p_0, \vec{p})) \\ &= \frac{1}{\pi}\,\mathrm{Im}D_H^R(p_0, \vec{p}) \\ D_H^{>(<)}(p_0, \vec{p}) &= \int \frac{d^4p}{(2\pi)^4} e^{ip\cdot x} D_H^{>(<)}(x_0, \vec{x})\end{aligned} \tag{1}$$

$$\begin{aligned}D_H^>(x_0, \vec{x}) &= \langle J_H(x_0, \vec{x}), J_H(0, \vec{0})\rangle \\ D_H^<(x_0, \vec{x}) &= \langle J_H(0, \vec{0}), J_H(x_0, \vec{x})\rangle, \qquad x_0 > 0.\end{aligned} \tag{2}$$

In the present paper we study local meson operators of the form

$$J_H(t, x) = \bar{q}(t, x)\Gamma_H q(t, x) \tag{3}$$

with

$$\Gamma_H = 1, \gamma_5, \gamma_\mu, \gamma_5\gamma_\mu, \gamma_\mu\gamma_\nu \tag{4}$$

for scalar, pseudoscalar, vector, axial-vector and tensor channels. The relation of these quantum number channels to different meson states is given in Table I.

The correlators $D_H^{>(<)}(x_0, \vec{x})$ satisfy the well-known Kubo-Martin-Schwinger (KMS) condition [22]

$$D_H^>(x_0, \vec{x}) = D^<(x_0 + i/T, \vec{x}). \tag{5}$$

Inserting a complete set of states and using Eq. (5), one gets the expansion

$$\begin{aligned}\sigma_H(p_0, \vec{p}) = \frac{(2\pi)^2}{Z}\sum_{m,n}(e^{-E_n/T} \pm e^{-E_m/T}) \\ \times \langle n|J_H(0)|m\rangle|^2\delta^4(p_\mu - k_\mu^n + k_\mu^m),\end{aligned} \tag{6}$$

where Z is the partition function, and $k^{n(m)}$ refers to the four-momenta of the state $|n(m)\rangle$.

A stable mesonic state contributes a δ function-like peak to the spectral function

$$\sigma_H(p_0, \vec{p}) = |\langle 0|J_H|H\rangle|^2\epsilon(p_0)\delta(p^2 - m_H^2), \tag{7}$$

where m_H is the mass of the state. For a quasiparticle in the medium one gets a smeared peak, with the width being the thermal width. As one increases the temperature, the width increases and at sufficiently high temperatures, the contribution from the meson state in the spectral function may be sufficiently broad so that it is not very meaningful to speak of it as a well-defined state any more. The spectral function as defined in Eq. (6) can be directly accessible by high energy heavy ion experiments. For example, the spectral function for the vector current is directly related to the differential thermal cross section for the production of dilepton pairs [23]

$$\left.\frac{dW}{dp_0 d^3p}\right|_{\vec{p}=0} = \frac{5\alpha_{\mathrm{em}}^2}{27\pi^2}\frac{1}{p_0^2(e^{p_0/T} - 1)}\sigma(p_0, \vec{p}). \tag{8}$$

Then presence or absence of a bound state in the spectral function will manifest itself in the peak structure of the differential dilepton rate.

In finite temperature lattice calculations, one calculates Euclidean time propagators, usually projected to a given spatial momentum

$$G_H(\tau, \vec{p}) = \int d^3x e^{i\vec{p}.\vec{x}}\langle T_\tau J_H(\tau, \vec{x})J_H(0, \vec{0})\rangle. \tag{9}$$

This quantity is an analytical continuation of $D^>(x_0, \vec{p})$

$$G_H(\tau, \vec{p}) = D^>(-i\tau, \vec{p}). \tag{10}$$

Using this equation and the KMS condition one can easily show that $G_H(\tau, \vec{p})$ is related to the spectral function,

TABLE I. Meson states in different channels

Γ	$^{2S+1}L_J$	J^{PC}	$u\bar{u}$	$c\bar{c}(n=1)$	$c\bar{c}(n=2)$	$b\bar{b}(n=1)$	$b\bar{b}(n=2)$
γ_5	$^1S_0$	0^{-+}	π	η_c	η_c'	η_b	η_b'
γ_s	$^3S_1$	1^{--}	ρ	J/ψ	ψ'	$\Upsilon(1S)$	$\Upsilon(2S)$
$\gamma_s\gamma_{s'}$	$^1P_1$	1^{+-}	b_1	h_c		h_b	
1	$^3P_0$	0^{++}	a_0	χ_{c0}		$\chi_{b0}(1P)$	$\chi_{b0}(2P)$
$\gamma_5\gamma_s$	$^3P_1$	1^{++}	a_1	χ_{c1}		$\chi_{b1}(1P)$	$\chi_{b1}(2P)$
		2^{++}		χ_{c2}		$\chi_{b2}(1P)$	$\chi_{b2}(2P)$

Eq. (1), by an integral equation (see e.g. appendix B of Ref. [11]):

$$G(\tau, \vec{p}) = \int_0^\infty d\omega \sigma(\omega, \vec{p}) K(\omega, \tau)$$
$$K(\omega, \tau) = \frac{\cosh(\omega(\tau - 1/2T))}{\sinh(\omega/2T)}. \quad (11)$$

This equation is the basic equation for extracting the spectral function from meson correlators. Methods to do this will be discussed in the next section. Equation (11) is valid in the continuum. Formally the same spectral representation can be written for the Euclidean correlator calculated on the lattice $G^{\mathrm{lat}}(\tau, \vec{p})$. The corresponding spectral function, however, will be distorted by the effect of the finite lattice spacing. These distortions have been calculated in the free theory [24,25].

III. BAYESIAN ANALYSIS OF MESON CORRELATORS

The obvious difficulty in the reconstruction of the spectral function from Eq. (11) is the fact that the Euclidean correlator is calculated only at $\mathcal{O}(10)$ data points on the lattice, while for a reasonable discretization of the integral in Eq. (11) we need $\mathcal{O}(100)$ degrees of freedom. The problem can be solved using Bayesian analysis of the correlator, where one looks for a spectral function which maximizes the conditional probability $P[\sigma|DH]$ of having the spectral function σ given the data D and some prior knowledge H (for reviews see [26,27]). Different Bayesian methods differ in the choice of the prior knowledge. One version of this analysis which is extensively used in the literature is the *maximum entropy method* (MEM) [28,29]. It has been used to study different correlation functions in quantum field theory at zero and finite temperature [15–17,26,29–41]. In this method the basic prior knowledge is the positivity of the spectral function and the prior knowledge is given by the Shannon-Janes entropy

$$S = \int d\omega \left[\sigma(\omega) - m(\omega) - \sigma(\omega) \ln\left(\frac{\sigma(\omega)}{m(\omega)}\right)\right].$$

The real function $m(\omega)$ is called the default model and parametrizes all additional prior knowledge about the spectral functions, e.g. such as the asymptotic behavior at high energy [26,29]. For this case the conditional probability becomes

$$P[\sigma|DH] = \exp\left(-\frac{1}{2}\chi^2 + \alpha S\right), \quad (12)$$

with χ^2 being the standard likelihood function and α a real parameter. In the existing MEM analysis of the meson spectral functions the Bryan's algorithm was used [28].

Here we will introduce a new algorithm described below. To maximize (12) we have to solve the following equation

$$\frac{\delta}{\delta\sigma(\omega)}\left[\frac{1}{2}\chi^2 - \alpha S\right] = 0. \quad (13)$$

If we perform N measurements at points $\tau_1, \ldots, \tau_N$ with results $\bar{G}_i$ $(i = 1 \ldots N)$, and the data model $G_i[\sigma]$ is described by (11), then we obtain

$$\sum_{i,j=1}^{N} K(\omega, \tau_i) C_{ij}^{-1} (G_j[\sigma] - \bar{G}_j) + \alpha \ln\frac{\sigma(\omega)}{m(\omega)} = 0, \quad (14)$$

where C_{ij} is the correlation matrix. With the notation

$$s_i \equiv -\frac{1}{\alpha}\sum_{j=1}^{N} C_{ij}^{-1}(G_j[\sigma] - \bar{G}_j)$$

we can write this equation as

$$\sigma(\omega) = m(\omega)\exp\left[\sum_{i=1}^{N} s_i K(\omega, \tau_i)\right]. \quad (15)$$

Since s_i itself depends on $\sigma(\omega)$, this is just a reparametrization of the original problem. However, by substituting back this form into (14) we obtain

$$\sum_{i=1}^{N} K(\omega, \tau_i)\left[\sum_{j=1}^{N} C_{ij}^{-1}(G_j[\sigma] - \bar{G}_j) + \alpha s_i\right] = 0. \quad (16)$$

Since the functions $K(\omega, \tau_i)$ are linearly independent, this equation can hold only if the expressions in the square brackets are zero. Multiplying by the correlation matrix it reads

$$\alpha\sum_{j=1}^{N} C_{ij} s_j + G_j[\sigma] - \bar{G}_j = 0. \quad (17)$$

Since the relation $\sigma[s]$ is known one can solve these equations.

We can go even a step further by recognizing that

$$G_j[\sigma] = \int_0^\infty d\omega K(\omega, \tau_j) m(\omega) e^{\sum_n s_n K(\omega, \tau_n)}$$
$$= \frac{\partial}{\partial s_j}\int_0^\infty d\omega m(\omega) e^{\sum_n s_n K(\omega, \tau_n)}$$
$$= \frac{\partial}{\partial s_j}\int_0^\infty d\omega \sigma(\omega). \quad (18)$$

This allows us to define a function

$$U = \frac{\alpha}{2}\sum_{i,j=1}^{N} s_i C_{ij} s_j + \int_0^\infty d\omega\sigma(\omega) - \sum_{i=1}^{N}\bar{G}_i s_i. \quad (19)$$

Using this function (17) can be written as

$$\frac{\partial U}{\partial s_i} = 0. \quad (20)$$

It can also be shown that $\partial^2 U/\partial s_i \partial s_j$ is positive definite. Therefore we reformulated the MEM problem to the task

of *minimizing U*. This is a minimization problem in number of data dimensions, which is not a more difficult task than applying a χ^2 method. So we should expect that our MEM-code runs as fast as a χ^2 code, as it is indeed the case. We used the Levenberg-Marquant method to perform the minimization which in most cases is stable enough to find the minimum.

It is worth to make connection between our method and the Bryan algorithm [28]. In both cases the true problem is number of data dimensional—in more dimensions the problem would be under-determined. To find the relevant subspace, the Bryan algorithm uses singular value decomposition, while we find the same relevant subspace by exact mathematical transformations. Although the method of identifying the subspace is different, the result is the same, and in both cases one proceeds with solving the original problem in this restricted subspace. The advantage of the new algorithm is that it is more stable numerically when we reconstruct quarkonium spectral functions at zero temperature. We will discuss this issue in more detail in Sec. V.

To demonstrate the reconstruction power of MEM and also to reveal the role of noise in the data we give some illustrative examples. We use the simple uncorrelated noise model

$$\delta G(\tau) = b\tau G(\tau), \tag{21}$$

and vary b. For the given spectral function we generate mock data for $N_\tau = 32$ time slices. The terms proportional to α introduce the dependence on the prior knowledge, so it is advantageous to choose for it smallest value possible; the typical value in the analysis was 10^{-8}–10^{-12}.

The first is a typical continuum spectral function consisting of a Dirac delta and a continuum part. In Fig. 1 the original spectral function can be seen together with the MEM-reconstruction in the presence and absence of noise, respectively, (the magnitude of the noise was $b = 10^{-4}$).

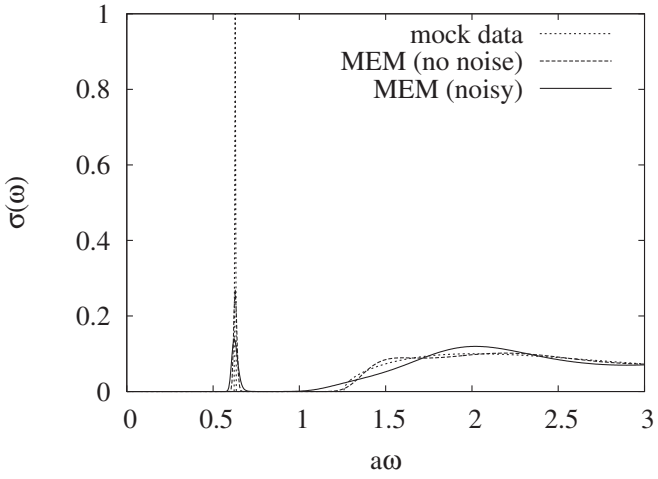

FIG. 1. The continuum-like spectral function and its MEM-reconstruction in presence and in absence of noise, respectively.

The matching is not perfect, but all the main characteristics are present. The ability of MEM to reconstruct finite width spectral functions has been demonstrated in a similar analysis with the Breit-Wigner ansatz used to model the ground state instead of the Dirac delta [21]. The simple noise model in this analysis assumes a diagonal correlation matrix. In real situations the correlation matrix is not diagonal. We will discuss this case later in the course of the analysis of the lattice correlators.

IV. LATTICE FORMULATIONS AND PARAMETERS FOR CHARMONIUM PHYSICS

To study the charmonium system at zero and finite temperature we use the anisotropic Fermilab formulation described in Ref. [42]. In our study we use the quenched approximation and use the standard Wilson action in the gauge sector for which the relation between the bare ξ_0 and the renormalized anisotropy $\xi = a_s/a_t$ is known in a wide range of the gauge coupling $\beta = 6/g^2$ [43]. For the heavy quarks we use the anisotropic clover action [42]

$$S_q^\xi = \sum_x \bar\psi(x)\Big[m_0 + \nu_t \not{D}_t^{\text{Wilson}} + \frac{\nu_s}{\xi_0}\sum_s \not{D}_s^{\text{Wilson}} - \frac{1}{2}\Big(C_{\text{sw}}^t \sum_s \sigma_{ts}F_{ts} + \frac{C_{\text{sw}}^s}{\xi_0}\sum_{s<s'}\sigma_{ss'}F_{ss'}\Big)\Big]\psi(x). \tag{22}$$

Here the Dirac operator is defined as

$$D_\mu^{\text{Wilson}} = \nabla_\mu - \frac{1}{2}\gamma_\mu\Delta_\mu, \tag{23}$$

with

$$\nabla_\mu\psi(x) = \frac{1}{2}[U_\mu(x)\psi(x+\mu) - U_\mu^\dagger(x-\mu)\psi(x-\mu)] \tag{24}$$

$$\Delta_\mu\psi(x) = [U_\mu(x)\psi(x+\mu) + U_\mu^\dagger(x-\mu)\psi(x-\mu) - 2\psi(x)]. \tag{25}$$

Furthermore, $\sigma_{\mu,\nu} = \{\gamma_\mu, \gamma_\nu\}$ and the field strength tensor is defined as

$$F_{\mu\nu}(x) = -\frac{i}{2}[Q_{\mu\nu} - Q_{\mu\nu}^\dagger] \tag{26}$$

$$\begin{aligned} 4Q_{\mu\nu}(x) = {} & U_\mu(x)U_\nu(x+\hat\mu)U_\mu^\dagger(x+\hat\nu)U_\nu^\dagger(x) \\ & + U_\nu(x)U_\mu^\dagger(x-\hat\mu+\hat\nu)U_\nu^\dagger(x-\hat\mu)U_\mu(x-\hat\mu) \\ & + U_\mu^\dagger(x-\hat\mu)U_\nu^\dagger(x-\hat\mu-\hat\nu) \\ & \times U_\mu(x-\hat\mu-\hat\nu)U_\nu(x-\hat\nu) + U_\nu^\dagger(x-\hat\nu) \\ & \times U_\mu(x-\hat\nu)U_\nu(x+\hat\mu-\hat\nu)U_\mu^\dagger(x). \end{aligned} \tag{27}$$

As in Ref. [42] we fix $\nu_s = 1$ and use tadpole-improved values for the clover coefficients. The remaining parameters of the action, the bare heavy quark mass m_0 and the

bare velocity of light ν_t are fixed nonperturbatively. The bare quark mass is fixed by requiring that either the pseudoscalar (η_c) mass or the spin averaged $1S$ mass are equal to the experimental value. To fix ν_t we study the dispersion relation $E(p)$ of η_c and require that the velocity of light defined by [42]

$$c = \frac{\sqrt{16E^2(p_1) - 15E^2(p_0) - E^2(p_2)}}{\sqrt{12}\Delta p} \qquad (28)$$
$$p_n = 2\pi n/N_s, \qquad \Delta p = 2\pi/N_s$$

is equal to one. Here N_s is the spatial size of the lattice. For crosscheck we also calculate the velocity of light given by the simpler definition

$$c = \frac{\sqrt{E^2(p_1) - E^2(p_0)}}{\Delta p}. \qquad (29)$$

Both definitions give consistent results. In our study we use $\xi = 2$, 4 and $\beta = 5.7$, 5.9, 6.1, 6.5 corresponding to temporal lattice spacings $a_t^{-1} = 1.905$–14.12 GeV. The bare anisotropy ξ_0 for a given renormalized anisotropy was calculated in Ref. [43] for $\beta = 5.5$–6.5. To set the scale for the lattice spacing we use the tradition phenomenological value $r_0 = 0.5$ fm for the Sommer scale [44]. The Sommer scale r_0 has also been calculated for anisotropic Wilson action for $\beta = 5.5$–6.1 [45]. For larger β values we use extrapolation based on RG inspired β function [46]

$$\frac{a_s}{r_0}(\beta) = \frac{1}{c_0} R(\beta)\left(1 + c_2\left[\frac{R(\beta)}{R(6)}\right]^2 + c_4\left[\frac{R(\beta)}{R(6)}\right]^4\right), \qquad (30)$$

with $R(\beta) = (b_0\beta)^{-b1/(2b_0^2)} \exp(-1/(2b_0)\beta)$ being the standard 2-loop beta function. The extrapolation is done for $\beta = 6.5$ using $\beta = 5.9$, 6.0 and 6.1. To crosscheck the results we also did the extrapolation including the point at $\beta = 5.8$ and the difference gives the estimate of the error on the extrapolated r_0. Alternatively one can estimate the lattice spacing from the difference between the mass of $^1P_1$ state and the spin averaged $1S$ mass: $\Delta M(^1P_1 - \overline{1S})$. To a very good approximation this mass difference is not affected by fine and hyperfine splitting and thus is not very sensitive to quenching errors. It was found that close to the continuum limit the lattice spacing determined from $\Delta M(^1P_1 - \overline{1S})$ is different from that determined from r_0 by 10% [42,47] if we use the phenomenological value $r = 0.5$ fm. Using the value of $r_0 = 0.469(7)$ determined in full QCD [48] would give a value for $\Delta M(^1P_1 - \overline{1S})$ splitting which is closer to the experimental one, however, the $\Delta M(\overline{2S} - \overline{1S})$ splitting would be even further away from the experimental value [47]. This problem is due to the quenched approximation. The parameters of simulations are summarized in Table II For $\xi = 2$ they are identical to those of Ref. [42]. For $\xi = 4$ the values of the clover coefficients have been taken from Ref. [49], and other two parameters, m_0 and ν_t were fixed nonperturbatively as described above.

By studying the large distance falloff of the correlators we determine the mass of the ground state in each quantum number channel. The pseudoscalar ground state masses from the fit are also given in Table II.

V. CHARMONIUM SPECTRAL FUNCTIONS AT ZERO TEMPERATURE

In this section we discuss the calculations of the charmonium spectral functions at zero temperature for different channels. The continuum meson current in Eq. (3), J_H is related to the lattice current as

$$J_H = Z_H a_s^3 \bar{\psi}\Gamma_H \psi, \qquad (31)$$

where ψ is the lattice quark field in Eq. (22). The renormalization constant Z_H can be calculated in perturbation theory or nonperturbatively. Unfortunately for anisotropic clover action they have not been calculated. Since in this

TABLE II. Simulation parameters for charmonium at zero temperature. Also shown here is the mass of the η_c state and the renormalized speed of light c.

β	5.7	5.9	6.1	6.1	6.5
$N_s^2 \times N_t$	$8^3 \times 64$	$16^3 \times 64$	$16^3 \times 64$	$16^3 \times 96$	$24^2 \times 32 \times 160$
(ξ, ξ_0)	(2,1.6547)	(2,1.6907)	(2,1.7183)	(4,3.2108)	(4,3.31655)
r_0/a_s	2.414(8)	3.690(11)	5.207(29)	5.189(21)	8.96(4)
a_t^{-1} [Gev]	1.905	2.913	4.110	8.181	14.12
$C_{\rm sw}^s$	2.138	1.889	1.7614	1.9463	1.7054
$C_{\rm sw}^t$	1.3252	1.2055	1.1431	1.0984	0.9002
m_0	0.51	0.195	0.05	0.05	−0.025
ν_t	1.01	1.09	1.12	1.25	1.19
$M(\eta_c)$ [GeV]	3.029(1)	3.052(1)	2.994(2)	2.983(3)	3.031(9)
$c(0)$	1.000(2)	0.984(3)	0.984(3)	1.002(4)	1.001(7)
L_s [fm]	1.66	2.17	1.54	1.54	1.34
configs	2000	1560	930	500	630

paper we are mainly interested in controlling systematic errors in the spectral functions and the temperature dependence of the charmonium correlators, the exact values of the renormalization constants are not important. Nonetheless, when we compare the spectral functions calculated at different lattice spacing in the plots it is convenient to take into account the effect of Z_H. We do this in an *ad hoc* way by choosing Z_H such that the continuum part of the spectral function is roughly equal to its free value at large energies. The values of Z_H are given in the Appendix. In what follows we will discuss charmonium spectral functions at zero spatial momentum $\vec{p} = 0$.

A. Pseudoscalar and vector spectral functions at zero temperature

In this subsection we discuss our results on charmonium spectral functions obtained using MEM. To reconstruct the spectral functions we used the algorithm described in Sec. III. We also compare the results with the Bryan algorithm for the pseudoscalar spectral function for $\beta = 6.1$, $\xi = 4$. The problem with the Bryan algorithm is that it does not work well for charmonium correlators if the time extent is sufficiently large, which is the case at low temperatures; the iterative procedure does not always converge. For instance at $\beta = 6.1$, $\xi = 4$ and $16^3 \times 96$ lattice we could get the spectral functions using the Bryan algorithm only when using $t_{\max} = 24$ data points in the time direction. With the new algorithm there is no restriction on $t_{\max}$ which can be as large as $N_t/2$. The comparison of the spectral functions obtained with the two algorithm is given in the Appendix.

When we analyze the correlation function using MEM we need two inputs: the default model $m(\omega)$ and the parameter α. Thus the spectral function we get depends both on α and the default model. We investigated the α dependence of the spectral functions. For sufficiently large α the spectral function is very smooth and shows no peaks. As we decrease α the spectral function shows more and more peaks. These features are also shown in the Appendix. It has been shown that one can construct the probability $P[\alpha|Dm]$ of having some α for given data and default model $m(\omega)$ [28,50]. Typically, for high statistics data this probability is a smooth function of α and has a maximum at some $\alpha = \alpha_{\max}$ [26,30]. To eliminate the α dependence the spectral functions calculated at fixed α were averaged over alpha with the weight $P[\alpha|Dm]$ [15–17,26,29,30]. In the present analysis we simply calculate the spectral function at $\alpha_{\max}$. In the new algorithm used in this paper the subspace, in which the search for the spectral function (i.e. the maximization of the conditional probability $P[\sigma|DH]$) is performed, is chosen by selecting different data on the correlator $G(t)$, $t = 0, 1, 2, \ldots, N_t/2$ which go into the analysis. Although the dimension of this subspace can be as large as $N_t/2$ in practice it is limited by statistics. In our analysis the dimension of this subspace was tuned to the largest possible value giving a smooth α-dependence of $P[\alpha|Dm]$ with a unique maximum. We use different type of default models, all of them being smooth function of ω, $m(\omega) = m_0\omega^2$, $m(\omega) = h =$ const as well as the form given by the free spectral function calculated on the lattice [24]. To reduce the sensitivity to the lattice artifacts at short time separation arising from anisotropy, in the reconstructed spectral function we do not include the data on the correlator for $t < \xi$ in our analysis. This was also done in Ref. [16]. It turns out, however, that including these points does not alter significantly the results.

The zero temperature spectral functions for three different lattice spacings are summarized in Fig. 2. Here we used the simple default model $m(\omega) = 1$ (in this paper we always give the default model in units of the spatial lattice spacing). To get a feeling for the statistical errors in the spectral functions we calculate its mean value in some interval I:

$$\bar{\sigma} = \frac{\int_I d\omega \sigma(\omega)}{\int_I d\omega}. \tag{32}$$

Then we calculated the error on $\bar{\sigma}$ using standard jackknife method. These errors are shown in Fig. 2, where the length of the intervals are shown as horizontal error bars. As one can see from the figure, the $\eta_c(1S)$ can be identified very well. The second peak is likely to correspond to excited states. Because of the heavy quark mass the splitting between different radial excitations is small and MEM cannot resolve different excitations individually but rather produces a second broad peak to which all radial excitation contribute. This can be seen from the fact that the amplitude of the second peak (i.e. the area under the peak) is more than 2 times larger than the first one. Physical considerations tell us that it should be smaller than the first

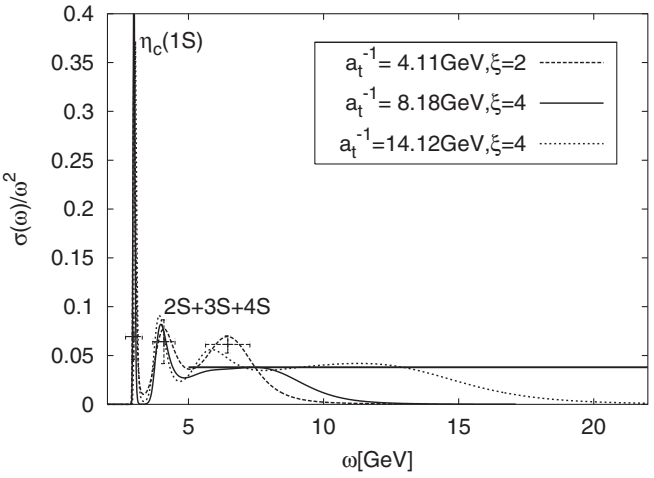

FIG. 2. The pseudoscalar spectral function at zero temperature for three finest lattice spacings. The horizontal line corresponds to the spectral function in the free massless limit at zero lattice spacing.

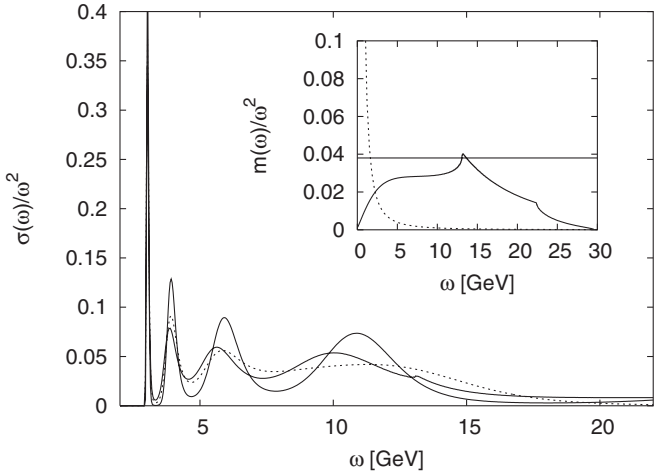

FIG. 3. The default model dependence of the pseudoscalar spectral function at the finest lattice spacing ($\beta = 6.5$). In the insertions the default models corresponding to different spectral functions are shown.

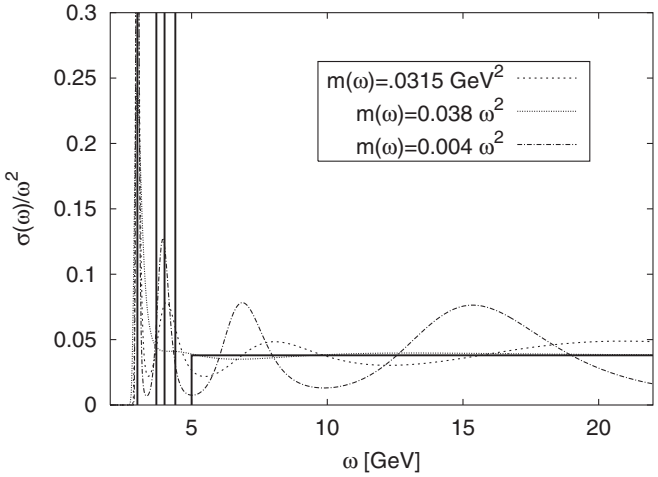

FIG. 4. The comparison of spectral functions obtained from MEM with the input spectral function (thick black lines).

amplitude if it was a $2S$ state. When comparing amplitudes and peak positions from MEM analysis and from double exponential fits we find very good agreement for the first peak and a fair agreement for the second peak. The details of this comparison are given in the appendix. This gives us confidence that at zero temperature charmonium properties can be reproduced well with MEM.

For energies larger than 5 GeV we probably see a continuum in the spectral functions which is distorted by finite lattice spacing. In particular the spectral function is zero above some energy which scales roughly as a_s^{-1}. Note that for $\omega < 5$ GeV the spectral function does not depend on the lattice spacing.

One should control how the result depends on the default model. In Fig. 3 we show the spectral function for three different default models. One can see that the default model dependence is significant only for $\omega > 5$ GeV. This is not surprising as there are very few time slices which are sensitive to the spectral functions at $\omega > 5$ GeV, while the first peak is well determined by the large distance behavior of the correlator.

We would like to know how well we can reconstruct the spectral function using MEM. To answer this question we consider a model spectral function consisting of four peaks and the perturbative continuum. We used semirealistic masses and amplitudes calculated from potential model [11]. From this spectral function we generated mock data for the correlator $G^{\mathrm{mock}}(i)$ at lattice spacing $a_t^{-1} = 14.12$ GeV and $N_t = 160$. The correlation matrix used in the analysis of this mock data was defined as

$$C_{ij}^{\mathrm{mock}} = \frac{C_{ij}}{G(i)G(j)} G^{\mathrm{mock}}(i) G^{\mathrm{mock}}(j). \tag{33}$$

Here C_{ij} and $G(i)$ are the correlation matrix and meson correlators calculated in the pseudoscalar channel on $24^2 \times 32 \times 160$ lattice at $\beta = 6.5$.

The result of the MEM analysis of this mock data are shown in Fig. 4, where the four delta functions and the continuum of the model spectral function are shown as thick black lines. The first peak is reproduced quite well. The three radial excitations show up as one broad peak. Indeed, the area under the second peak is 1.05 GeV^3 while the input was 1.20 GeV^3. The continuum is only reproduced correctly when the default model has exactly the same form as the continuum at large ω.

So far we only discussed the pseudoscalar channel. We also calculated the spectral function in the vector channel defined as

$$\sigma_V(\omega) = \frac{1}{3}\sum_i \sigma_{ii}(\omega). \tag{34}$$

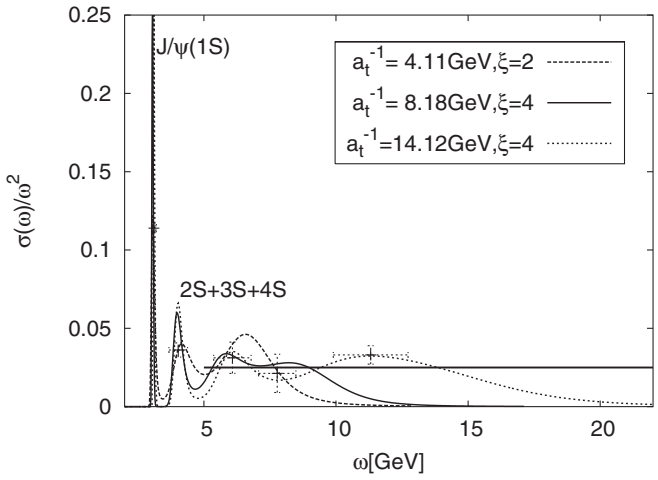

FIG. 5. The vector spectral function at zero temperature for three finest lattice spacings. The horizontal line is the spectral function in the free massless limit.

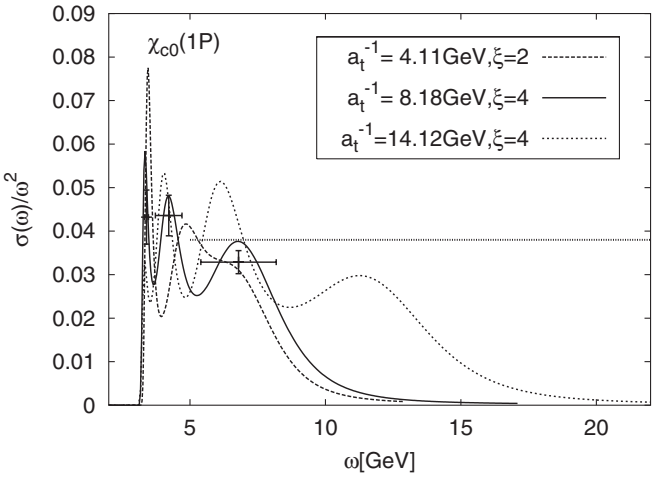

FIG. 6. The scalar spectral function at zero temperature for three finest lattice spacings.

The zero temperature vector spectral functions are shown in Fig. 5 for the three finest lattice spacings. The conclusions which can be derived from this figure are similar to the ones discussed above for the pseudoscalar channel. The first peak corresponds to the $J/\psi(1S)$ state, the second peak most likely is a combination of $2S$ and higher excited states, finally there is a continuum above 5 GeV which is, however, distorted by lattice artifacts. The similarity between the pseudoscalar and vector channel is, of course, expected. The lower lying states in theses channels differ only by small hyperfine splitting.

B. Spectral functions for P states

We calculated the spectral functions in the scalar, axial-vector and tensor channels which have the $1P$ charmonia as the ground state. The scalar spectral functions reconstructed using MEM are shown in Fig. 6. The first peak corresponds to χ_{c0} state, but it is not resolved as well as the ground state in the pseudoscalar channel. This is because the scalar correlator is considerably more noisy than the pseudoscalar or vector correlator. For the two finest lattice spacings there is a second peak which may correspond to a combination of excited P states. Above $\omega > 5$ GeV we see a continuum which is strongly distorted by lattice artifacts and probably also by MEM. In the Appendix we show the comparison of the amplitudes and the masses of the ground state from MEM and two exponential fits.

The spectral functions in the axial-vector and tensor channels are shown in Fig. 7. They look similar to the scalar spectral functions. As in the scalar channel the first peak is less pronounced than in the case of S wave charmonium spectral functions, and it corresponds to χ_{c1} and h_c state, respectively. The continuum part of the spectral function is again strongly distorted.

VI. CHARMONIUM CORRELATORS AT FINITE TEMPERATURE

As we have seen in the previous section the reconstruction of the spectral functions from lattice correlators is difficult already at zero temperature. At finite temperature it is even more difficult to control the systematic errors in the spectral functions reconstructed from MEM. This is because with increasing temperature the maximal time extent $\tau_{\max}$ is decreasing as $1/T$. Also the number of data points available for the analysis becomes smaller. Therefore we are looking for a method which can give some information about the change of the spectral functions as the temperature is increasing. The temperature dependence of the spectral function will manifest itself in the temperature dependence of the lattice correlator $G(\tau, T)$. Looking at Eq. (11) it is easy to see that the temperature dependence of $G(\tau, T)$ comes from the temperature dependence of the spectral function $\sigma(\omega, T)$ and the temperature dependence of the kernel $K(\tau, \omega, T)$. To separate out the trivial temperature dependence due to $K(\tau, \omega, T)$ following Ref. [17] we calculate the reconstructed correlator

$$G_{\text{recon}}(\tau, T) = \int_0^\infty d\omega \sigma(\omega, T = 0) K(\tau, \omega, T). \quad (35)$$

If the spectral function does not change with increasing temperature we expect $G(\tau, T)/G_{\text{recon}}(\tau, T) = 1$. In this section we are going to study the temperature dependence of this ratio for different channels at different lattice spacings. To fix the temperature scale we use the β depen-

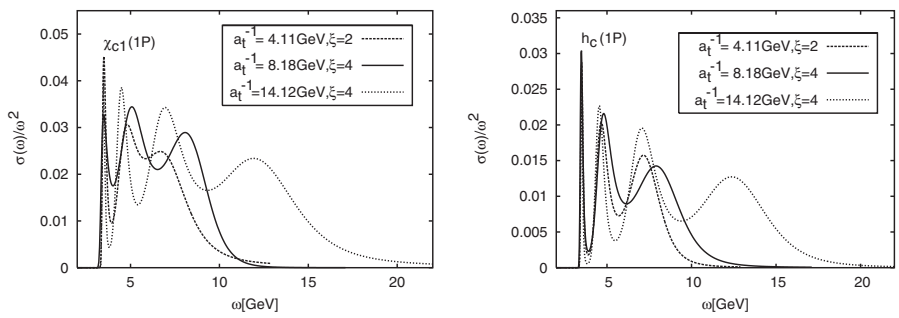

FIG. 7. The axial-vector (top) and tensor (bottom) spectral functions at zero temperature for three lattice spacings.

TABLE III. Simulation parameters for charmonium at finite temperature. We assumed $r_0 T_c = 0.7498(50)$ corresponding to $T_c = 295(2)$ MeV.

$\beta = 5.7$, $\xi = 2$			$\beta = 5.9$, $\xi = 2$			$\beta = 6.1$, $\xi = 2$			$\beta = 6.1$, $\xi = 4$			$\beta = 6.5$, $\xi = 4$		
lattice	T/T_c	#config	lattice	T/T_c	#config	lattice	T/T_c	#config	lattice	T/T_c	#config	lattice	T/T_c	#config
$8^3 \times 6$	1.08	500	$16^3 \times 16$	0.62	1000	$16^3 \times 24$	0.58	1000	$16^3 \times 32$	0.87	220	$24^3 \times 44$	1.09	110
			$16^3 \times 8$	1.23	1000	$16^3 \times 12$	1.16	250	$16^3 \times 26$	1.07	400	$24^3 \times 40$	1.20	1680
									$16^3 \times 24$	1.16	2010	$24^2 \times 32 \times 32$	1.50	1000
									$24^3 \times 20$	1.39	1900	$24^3 \times 24$	1.99	300
									$16^3 \times 16$	1.73	1000	$24^3 \times 20$	2.39	640
									$16^3 \times 12$	2.31	3000	$24^3 \times 16$	2.99	310
									$24^3 \times 24$	1.16	2040			

dence of the r_0 given by Eq. (30) and the value $r_0 T_c = 0.7498(50)$ [51] for the transition temperature T_c. The parameters of our finite temperature simulations are given in Table III.

A. The pseudoscalar correlators

First let us examine the temperature dependence of the pseudoscalar correlators. In Fig. 8 we show our numerical results for $G/G_{\rm recon}$ on coarse lattices with $\xi = 2$. The figure shows very little temperature dependence of the correlators till temperatures $1.2T_c$. Calculations at smaller lattice spacings enable us to consider higher temperatures. In Fig. 9 we show the temperature dependence of $G/G_{\rm recon}$ on our $\xi = 4$ lattices. We see very little change in the pseudoscalar correlator till temperatures as high as $1.5T_c$. Medium modifications of the correlator slowly turn on as we increase the temperature above this value. From the figures it is clear that the temperature dependence of the correlators is not affected significantly by the finite lattice spacing. The very small temperature dependence of the pseudoscalar correlator suggests that the corresponding ground state $\eta_c(1S)$ survives till temperatures as high as $1.5T_c$. The temperature dependence of the correlator found in this study is similar to that of Ref. [17] where isotropic lattices with very small lattice spacings, $a^{-1} = 4.86$, 9.72 GeV have been used. We find a somewhat stronger temperature dependence of $G/G_{\rm recon}$ than in Ref. [17]. In particular, at $1.5T_c$ we see small, but statistically significant deviations of $G/G_{\rm recon}$ from unity. At higher temperatures the deviation of $G/G_{\rm recon}$ from unity become slightly larger than those found in Ref. [17]. This is possibly due to the fact that cut-off effects are more important at higher temperatures. Thus despite similarities of the temperature dependence of the pseudoscalar correlator to findings of Ref. [17] we see quantitative differences. One should note, however, statistical errors and systematic uncertainties are larger in the analysis presented in Ref. [17] than in this calculation. The ratio $G/G_{\rm recon}$ starts to depend more strongly on the temperature around $2T_c$. This may suggest some quantitative differences in the properties of the lowest state at this temperature.

B. The *P*-wave correlators

In this subsection we are going to discuss the temperature dependence of the scalar, axial-vector and tensor correlators corresponding to P-states. The numerical re-

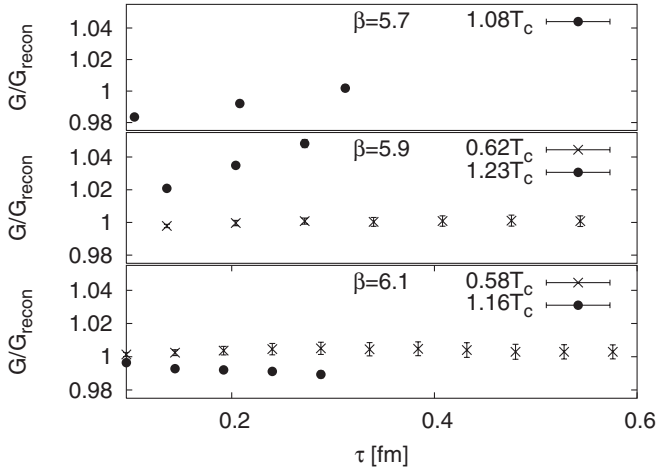

FIG. 8. The ratio $G/G_{\rm recon}$ for the pseudoscalar channel on coarse $\xi = 2$ lattices.

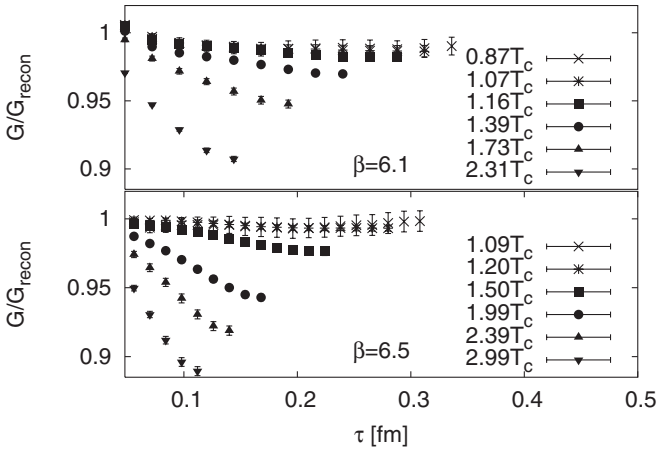

FIG. 9. The ratio $G/G_{\rm recon}$ for the pseudoscalar channel for the two finer $\xi = 4$ lattices.

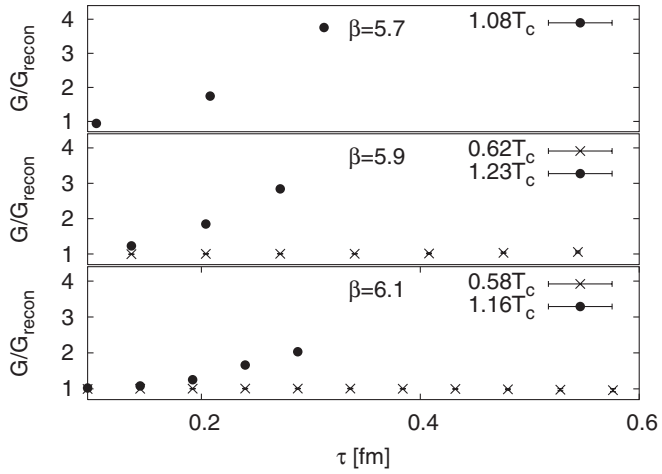

FIG. 10. The ratio G/G_{recon} for the scalar channel on coarse $\xi = 2$ lattices.

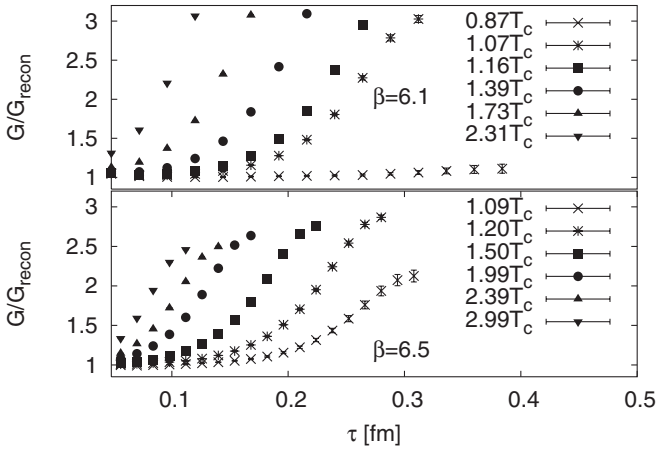

FIG. 12. The ratio G/G_{recon} for the axial-vector channel for $\xi = 4$ lattices.

sults for the scalar correlator on our $\xi = 2$ coarse lattices are shown in Fig. 10. As one can see the correlator is temperature independent below T_c and strongly enhanced above T_c. The magnitude of the enhancement is largest on the coarsest lattice and decreases with decreasing lattice spacing. The numerical results on fine lattices are shown in Fig. 11. We see some differences in G/G_{recon} calculated at $\beta = 6.1$ and $\beta = 6.5$. Thus the cut-off dependence of G/G_{recon} is larger in the scalar channel than in the pseudoscalar one. For $\beta = 6.1$ and $\xi = 4$ we also did calculations on $24^3 \times 24$ lattice to check finite volume effects. The corresponding results are shown in Fig. 11 indicating that the finite volume effects are small. On the finest lattice the enhancement of the scalar correlator is very similar to that found in calculations done on isotropic lattices [17], but small quantitative differences can be identified.

In Figs. 12 and 13 we show the temperature dependence of the axial-vector and tensor correlators, respectively, for $\xi = 4$. Qualitatively their behavior is very similar to the scalar correlator but the enhancement over the zero temperature result is larger. The results for the axial-vector correlators again are very similar to those published in Ref. [17]. The difference in G/G_{recon} calculated at $\beta = 6.1$ and $\beta = 6.5$ are smaller than in the scalar channel.

The large increase in the scalar, axial-vector and tensor correlators indicates strong modification of the corresponding spectral function and, possibly the dissolution of $1P$ charmonia states.

C. The vector correlator

The numerical results on the vector correlator are shown in Fig. 14 for $\xi = 4$. As one can see from the figures the temperature dependence of G/G_{rec} is different from the pseudoscalar case and this ratio is larger than unity for all lattice spacings. Though this appears to be surprising at first glance it can be explained by the presence of the diffusion pole in the vector spectral function [11,52]. Since the vector current is conserved there is a low energy

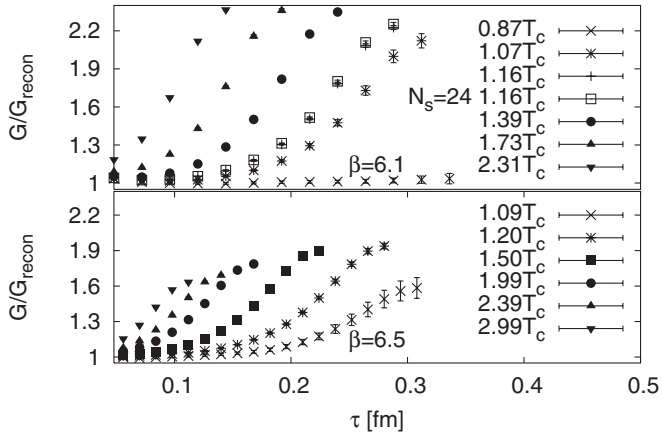

FIG. 11. The ratio G/G_{recon} for the scalar channel for the two finer $\xi = 4$ lattices.

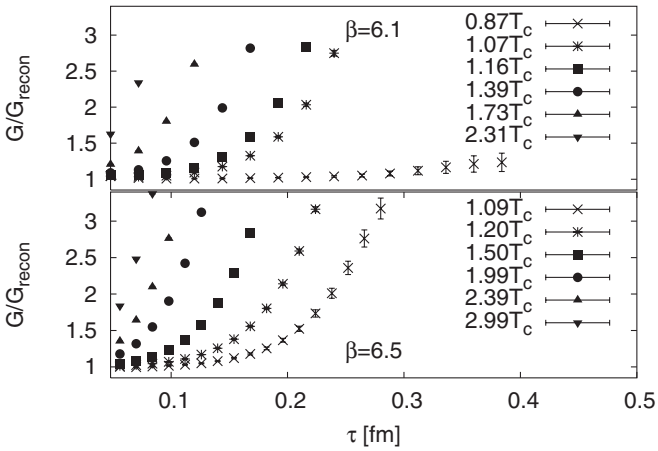

FIG. 13. The ratio G/G_{recon} for the tensor channel for $\xi = 4$ lattices.

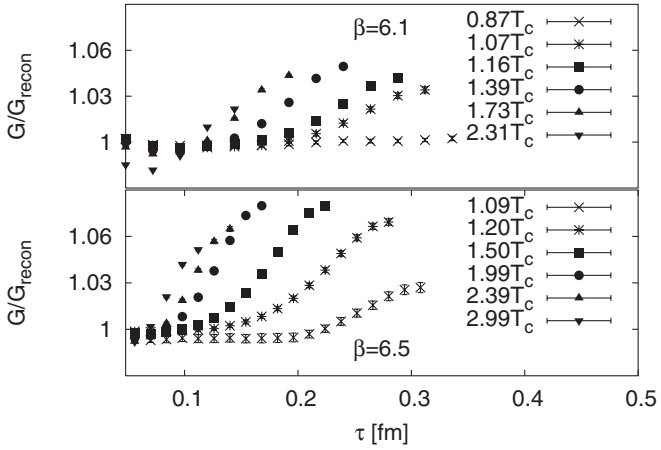

FIG. 14. The ratio G/G_{recon} for the vector channel for the two finer $\xi = 4$ lattices.

contribution in the vector spectral function at finite temperature

$$\sigma^V_{ii}(\omega \ll T) = \chi_s(T)\langle v^2_{\mathrm{th}}\rangle \omega \delta_\eta(\omega) \tag{36}$$

$$\sigma^V_{00}(\omega \ll T) = -\chi_s(T)\omega\delta(\omega), \tag{37}$$

where $\langle v^2_{\mathrm{th}}\rangle$ is the average thermal velocity of the heavy quark. For free streaming heavy quarks at temperature T we have $\langle v^2_{\mathrm{th}}\rangle = T/M$, with M being the heavy quark mass. Furthermore, $\chi_s(T)$ is the quark number susceptibility corresponding to the heavy quark, which in the noninteracting case is given by

$$\chi_s(T) = \frac{1}{T}\int \frac{d^3p}{(2\pi)^3}\frac{1}{\exp((\sqrt{p^2+M^2})/T)+1}. \tag{38}$$

The low energy parts of σ^V_{00} and σ^V_{ii} correspond to charge fluctuations and heavy quark diffusion, respectively. The smeared delta function, $\delta_\eta(\omega)$, in Eq. (36) carries information about the heavy quark diffusion constant D [52]. Using effective Langevin theory [52] it can be shown that

$$\delta_\eta(\omega) = \frac{1}{\pi}\frac{\eta}{\omega^2+\eta^2}, \qquad \eta = \frac{T}{MD}. \tag{39}$$

Therefore a very precise calculation of the vector correlator at finite temperature can provide some information about heavy quark transport in quark gluon plasma. This would require a method which is capable to isolate reliably the low energy contribution given to the Euclidean correlator which is given by Eq. (36). In the present paper we attempted to do so by subtracting from the finite temperature spectral functions the corresponding high energy part. We have assumed that this high energy part can be approximated reasonably well by the zero temperature spectral function. As we have seen in the previous subsection the pseudoscalar correlators show little temperature dependence up to temperatures as high as $1.5T_c$. This suggests that to some extent the spectral function up to this temperature can be approximated by the zero temperature spectral function. Since the lowest lying states in the pseudoscalar and vector channel are the same (up to the small hyperfine splitting) we may expect that the same is true for the vector channel, and that the only difference is the transport peak at $\omega \simeq 0$. Therefore we expect that $G^V - G^V_{\mathrm{recon}}$ should give an estimate for the low energy contribution coming from Eq. (36). It is easy to see that for the temporal component of the vector correlator we have $G_{00} = -T\chi_s(T)$ (c.f. Eq. (37)). This is a consequence of charge conservation. In Fig. 15 we show $-(G^V(\tau) - G^V_{\mathrm{recon}}(\tau))/G_{00}$ as function of τ. Note that this quantity does not depend on the renormalization constant. Since the width of the smeared delta function in Eq. (36) is small the above quantity should be approximately independent of τ and give the averaged thermal velocity $\langle v^2_{\mathrm{th}}\rangle$. The data in Fig. 15 do not agree completely with these expectations, deviations from this behavior are seen at short distances. The deviations are significant for $1.5T_c$. The problem is that with increasing temperature the high energy part of the spectral function starts to deviate from the zero temperature result, e.g. the properties of the lowest state could be slightly modified. The difference $G^V(\tau) - G^V_{\mathrm{recon}}(\tau)$ can be quite sensitive to these small changes, especially as the temperature increases.

It has been noticed already in the previous subsection that at $1.5T_c$ we see small but significant temperature modifications of the ratio G/G_{recon} for the pseudoscalar channel. Therefore at this temperature we attempted to take into account possible modifications of the high energy part of the spectral function. We do this by lowering the amplitude of the 1st peak by 7% in the zero temperature spectral function. In the pseudoscalar channel this ensures

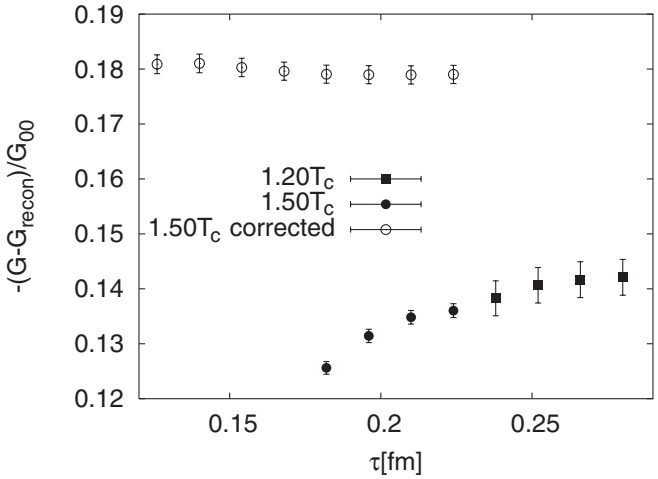

FIG. 15. The ratio $(G - G_{\mathrm{recon}})/G_{00}$ for the vector channel at $1.2T_c$ and $1.5T_c$. The open symbols show the same quantity at $1.5T_c$ where the possible modifications of the high energy part of the finite temperature spectral functions have been taken into account (see text).

that $G/G_{\rm recon}$ stays around unity. Using this modified spectral function in the vector channel we construct the quantity $-(G^V(\tau) - G^V_{\rm recon}(\tau))/G_{00}$ again. This is also shown in Fig. 15 as open symbols. We see that as a result of this correction $-(G^V(\tau) - G^V_{\rm recon}(\tau))/G_{00}$ shows a nice plateau and also increases with the temperature as expected. For the averaged thermal velocity squared we estimate $\langle v^2_{\rm th}\rangle \simeq 0.13$ for $1.2T_c$ and $\langle v^2_{\rm th}\rangle \simeq 0.18$ for $1.5T_c$. A nonzero diffusion coefficient η would produce a small curvature in $-(G^V(\tau) - G^V_{\rm recon}(\tau))/G_{00}$, clearly within present systematic uncertainties we cannot make any statement on the value of η.

The quantity $(G - G_{\rm recon})/G_{00}$ gives an estimate of T/M and is shown in Fig. 15. As one can see from the figure it has the expected magnitude.

VII. CHARMONIUM SPECTRAL FUNCTIONS AT FINITE TEMPERATURE

The study of the temperature dependence of the charmonium correlators presented in the previous section provides some useful insight into the properties of the spectral functions in the deconfined phase. In particular it suggests the survival of the $1S$ state till temperatures as high as $1.5T_c$ and significant modification or dissolution of the $1P$ charmonium states. To get more detailed information about charmonium spectral functions we would like to use MEM. We attempted to reconstruct the charmonium spectral functions at finite temperature on our two finest lattices. Below we are going to present our results for charmonium spectral functions at finite temperature for different channels.

A. Pseudoscalar and vector spectral functions at finite temperature

In Sec. V we have seen that using MEM we can reconstruct well the main features of the spectral function, in particular, the ground state properties. At finite temperature the situation becomes worse because the temporal extent is decreasing. The maximal time separation is $\tau_{\rm max} = 1/(2T)$. As a consequence it is no longer possible to isolate the ground state well. Also the number of available data points becomes smaller. While the later limitation can be overcome by using finer and finer lattice spacing in time direction the former limitation is always present. Therefore we should investigate systematic effects due to limited extent of the temporal direction. It appears that the pseudoscalar channel is the most suitable case for this investigation as at zero temperature it is well under control and there is no contribution from heavy quark transport. To estimate the effect of limited temporal extent we have calculated the spectral functions at zero temperature considering only the first $N_{\rm data}$ time slices in the analysis for $\beta = 6.5$, $\xi = 4$. The result of this calculation is shown in Fig. 16 where we considered $N_{\rm data} = 80$, 40, 20 and 16. The last two values correspond to our finite temperature

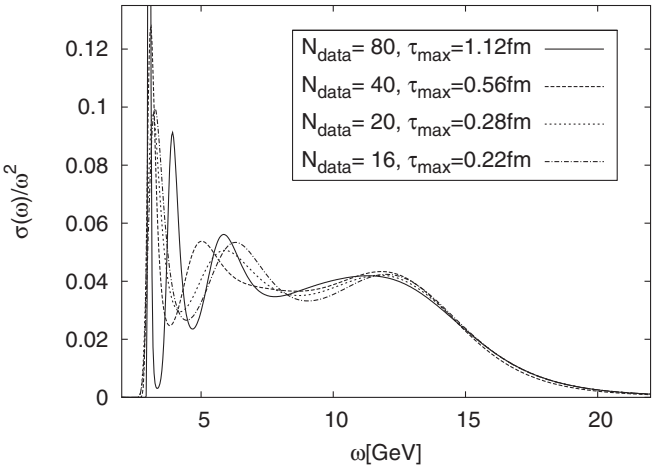

FIG. 16. The dependence of the reconstructed pseudoscalar spectral function on the maximal temporal extent for $\beta = 6.5$. In the analysis the default model $m(\omega) = 1$ has been used.

lattices at this value of β. In this case we see the first peak quite clearly when $\alpha = \alpha_{\rm max}$. For $\beta = 6.1$ as well as for $\beta = 6.5$ and $T > 1.5T_c$ the 1st peak is only clearly visible when we consider values for α which are smaller than $\alpha_{\rm max}$. As one can see from the figure already for $N_{\rm data} = 40$ and $\tau_{\rm max} = 0.56$ fm the second peak corresponding to radial excitation is no longer visible and the first peak becomes significantly broader. The position of the first peak, however, is unchanged. As the number of data points is further decreased ($N_{\rm data} = 20$, 16) we see further broadening of the first peak and a small shift of the peak position to higher energies. These systematic effects should be taken into account when analyzing the spectral functions at finite temperature. Therefore when studying the spectral functions at finite temperature we always compare with the zero temperature spectral functions reconstructed with the same number of data points and $\tau_{\rm max}$ as available at that temperature.

In Fig. 17 the spectral functions at different temperatures are shown together with the zero temperature spectral functions. We used $m(\omega) = 0.01$ as a default model for $T = 1.2T_c$ and $T = 1.5T_c$. For $T = 2.0T_c$ we used $m(\omega) = 1$ since the use of $m(\omega) = 0.01$ resulted in multiple maxima for $P[\alpha|DH]$. The figure shows that the pseudoscalar spectral function is not modified till $1.5T_c$ within the errors of our calculations. This is consistent with the conclusions of Ref. [16,17]. One should note, however, that it is difficult to make any conclusive statement based on the shape of the spectral functions as this was done in the above mentioned works. The dependence of the reconstructed spectral functions on the default model $m(\omega)$ is much stronger at finite temperature. We have reconstructed the spectral functions using different type of default models. For all temperatures $T \leq 1.5T_c$ the difference between the finite temperature spectral function and the zero temperature one is very small compared to the statistical errors

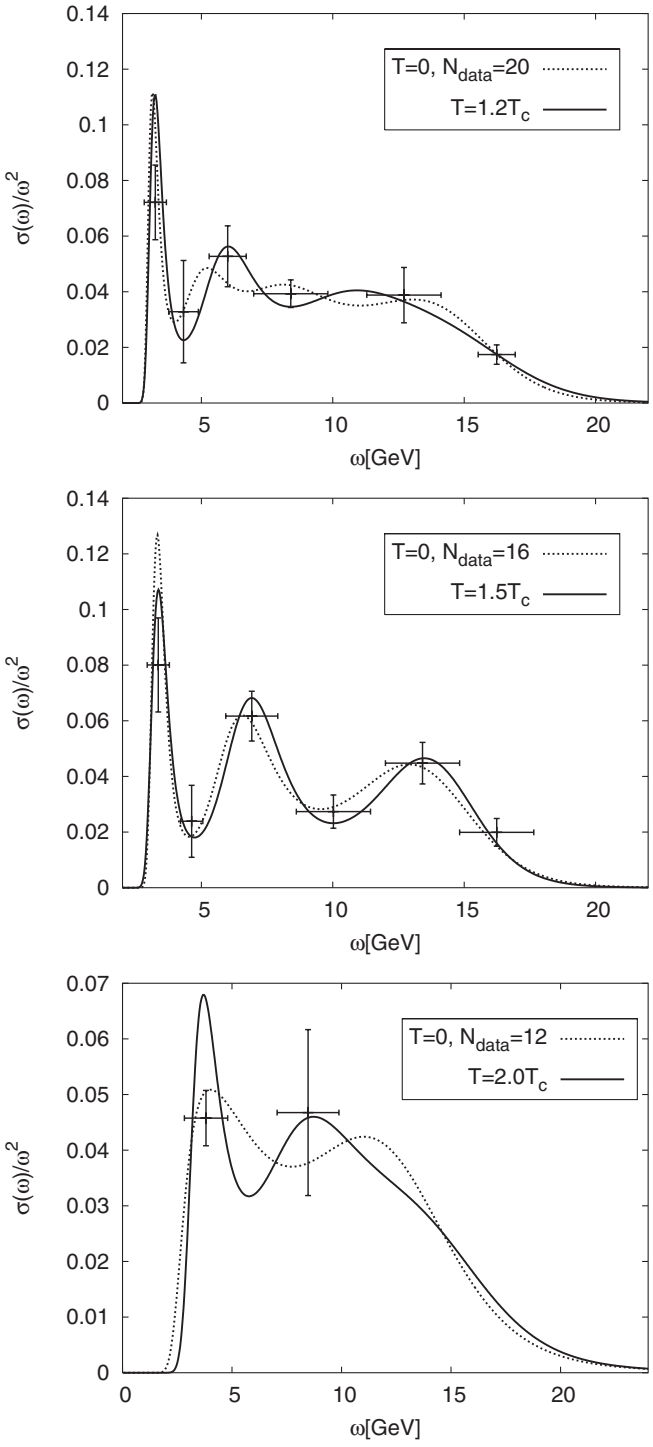

FIG. 17. The pseudoscalar spectral function for $\beta = 6.5$ and $N_t = 40, 32, 20$ corresponding to temperatures $1.2T_c$, $1.5T_c$ and $2.4T_c$. In the analysis the default model $m(\omega) = 0.01$ has been used for $1.2T_c$ and $1.5T_c$, while for $2.0Tc$ we used $m(\omega) = 1$.

for all default model considered here. We discuss this further in the Appendix. In particular we used the default model constructed from the high energy part of the lattice spectral functions calculated at zero temperature as this was done in Ref. [17]. The idea is that at sufficiently high energy the spectral function is dominated by the continuum and is temperature independent and is suitable to provide the prior knowledge, i.e. the default model. This behavior of $m(\omega)$ is then matched to a simple ω^2 dependence [17]. With this default model we have calculated the spectral function also at $\beta = 6.1$ on $16^3 \times 26$ and $16^3 \times 24$ lattices corresponding to $1.07T_c$ and $1.16T_c$. Also here we have found very little temperature dependence of the spectral functions. The survival of the $1S$ charmonium state was also confirmed by the analysis of the correlation functions with different spatial boundary condition [53].

At sufficiently high temperatures $1S$ charmonium states should dissolve and thus we expect significant changes in the spectral functions. The analysis of the pseudoscalar correlators suggests that this may happen around $2T_c$ which was also the conclusion of Ref. [16]. The spectral function at $T = 2.0T_c$ shown in Fig. 17 shows significant deviation from the zero temperature spectral function. However, this conclusions could be premature, since for a different default model, namely, the free lattice spectral function, we see almost no temperature dependence of the

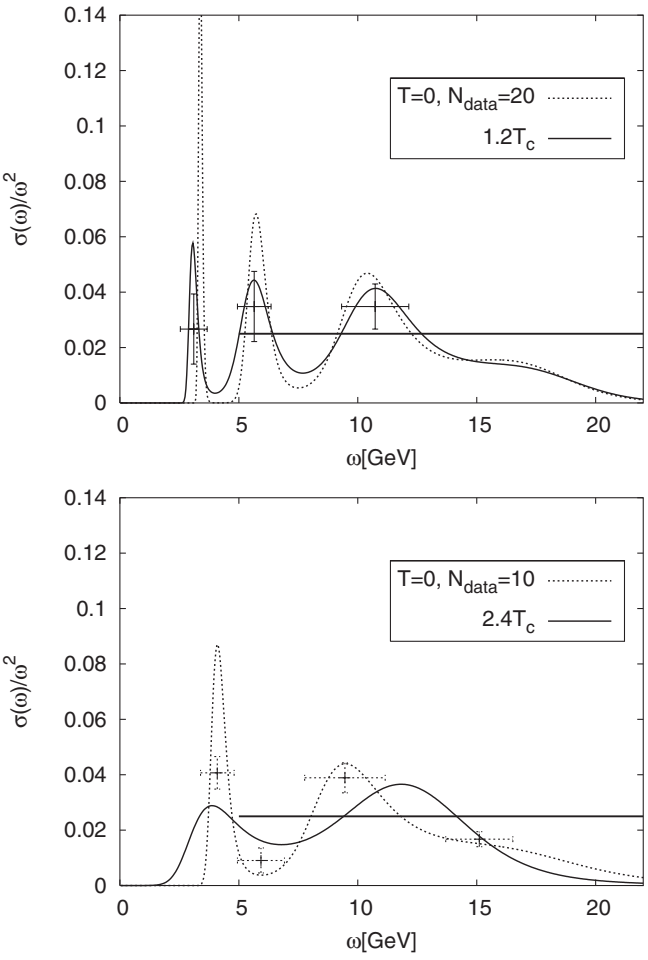

FIG. 18. The vector spectral function for $\beta = 6.5$ and $N_t = 40, 20$ corresponding to temperatures $1.2T_c$ and $2.4T_c$. In the analysis the default model $m(\omega) = 0.01$ has been used.

spectral function also at $2T_c$. Using the high energy part of the zero temperature spectral function as the default model as discussed above we arrive at a similar conclusion. Thus further studies are needed to establish at which temperature the $1S$ charmonia states dissolve.

We also calculated the spectral function in the vector channel. The results are shown in Fig. 18 for the default model $m(\omega) = 0.01$. As this was already discussed in the previous section the basic difference between the pseudoscalar and vector spectral functions at finite temperature is the presence of the transport peak at $\omega \simeq 0$. The difference of the temperature dependence of the vector and pseudoscalar correlators is consistent with this assumption. The vector spectral function reconstructed with MEM shows no evidence of the transport peak at $\omega \simeq 0$. On the other hand the spectral function at $1.2T_c$ differs from the zero temperature spectral function, in particular, the first peak is shifted to smaller ω values. We believe this is a problem of the MEM analysis which cannot resolve the peak at $\omega \simeq 0$ but instead mimics its effect by shifting the J/ψ peak to smaller ω. Also at $2.4T_c$ the spectral function extends to smaller ω values than in the pseudoscalar correlator which again indicates some structure at $\omega \simeq 0$. We analyzed the vector spectral functions using other choices for the default model and always found that the spectral functions at finite temperature differs from the zero temperature spectral functions and extend to significantly smaller ω values.

B. The *P*-wave spectral functions

We have studied the spectral functions in the scalar, axial-vector and tensor channels. Already at zero temperature the calculations of the P-wave spectral functions turned out to be much more difficult than for the S-wave spectral functions. This is even more the case at finite temperature where the number of data points is limited.

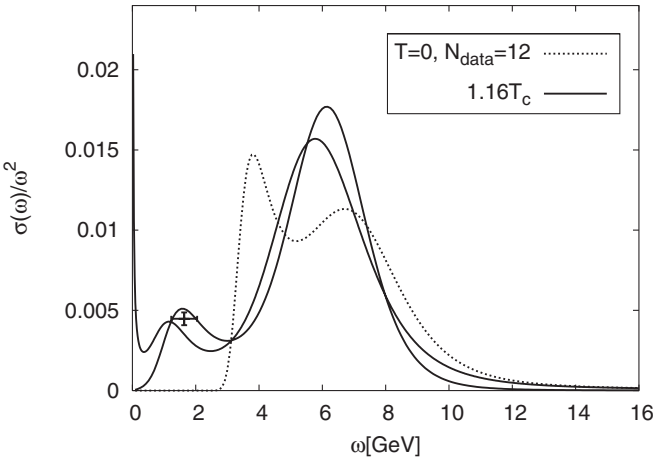

FIG. 19. The scalar spectral function for $\beta = 6.1$ at $T = 1.16T_c$ and at zero temperature reconstructed using $N_{\text{data}} = 12$. At finite temperature two default models $m(\omega) = 0.01$ and $m(\omega) = 0.038\omega^2$ have been used.

For most of the choices of the default model we have found that $P[\alpha|DH]$ has multiple maxima for all of our data sets. This is a sign of insufficient statistics. The only exception is the data set corresponding to $16^3 \times 24$ lattice with $\beta = 6.1$, i.e. $T = 1.16T_c$. The spectral function in the scalar channel for $\beta = 6.1$ at $T = 1.16T_c$ is shown in Fig. 19 and compared with spectral functions at zero temperature reconstructed using $N_{\text{data}} = 12$ data points. At finite temperature two default models, $m(\omega) = 0.038$ and $m(\omega) = 0.01$ have been used. We see that the spectral function at finite temperature is significantly modified compared to the zero temperature spectral function; its shape at small ω, however, strongly depends on the default model. We also analyzed the spectral function for these data with the default model constructed from the high energy part of the zero temperature lattice spectral functions as described in the previous subsection. The spectral functions obtained from this analysis are similar to those shown in Fig. 19 (see Appendix).

From the analysis of the spectral functions we conclude that the $1P$ states are dissociated in the deconfined phase at temperatures $T \simeq 1.1 - 1.2T_c$. This is consistent with the analysis of the correlators presented in the previous section as well as with the conclusions of Ref. [17]. On the other hand with present level of statistical accuracy we cannot make precise statements about the form of the P-wave spectral function at high temperatures.

VIII. CHARMONIUM CORRELATORS AND SPECTRAL FUNCTIONS AT FINITE MOMENTA

So far we considered charmonia at zero spatial momentum, i.e. charmonia at rest in the heatbath's rest frame. It is certainly of interest to study the temperature dependence of correlators and spectral functions at nonzero spatial momentum. Such a study has been done using isotropic lattices with lattice spacing $a^{-1} = 4.86$ GeV and 9.72 GeV [17,54]. It has been found that the pseudoscalar correlators are enhanced compared to the zero temperature correlators for nonvanishing spatial momenta. We have calculated the finite momentum pseudoscalar correlators at $\beta = 6.1$, $\xi = 4$ for different temperatures. The results are shown in Fig. 20. We see that the temperature dependence of G/G_{recon} at zero and finite momentum are different. At zero momentum this ratio decreases monotonically with increasing τ and increasing temperature. At finite momentum this is not the case, we see that the decrease in G/G_{recon} is at least weaker, and at sufficiently large momenta we see even that this ratio increases with τ. The differences in G/G_{recon} calculated in this work and in Refs. [17,54] are present already at zero momentum and are presumably due to finite lattice spacing errors. Apart from this the momentum dependence of the pseudoscalar correlators is similar to the findings of Refs. [17,54]. We also calculated the spectral function at finite temperature and found that the temperature dependence of the pseudo-

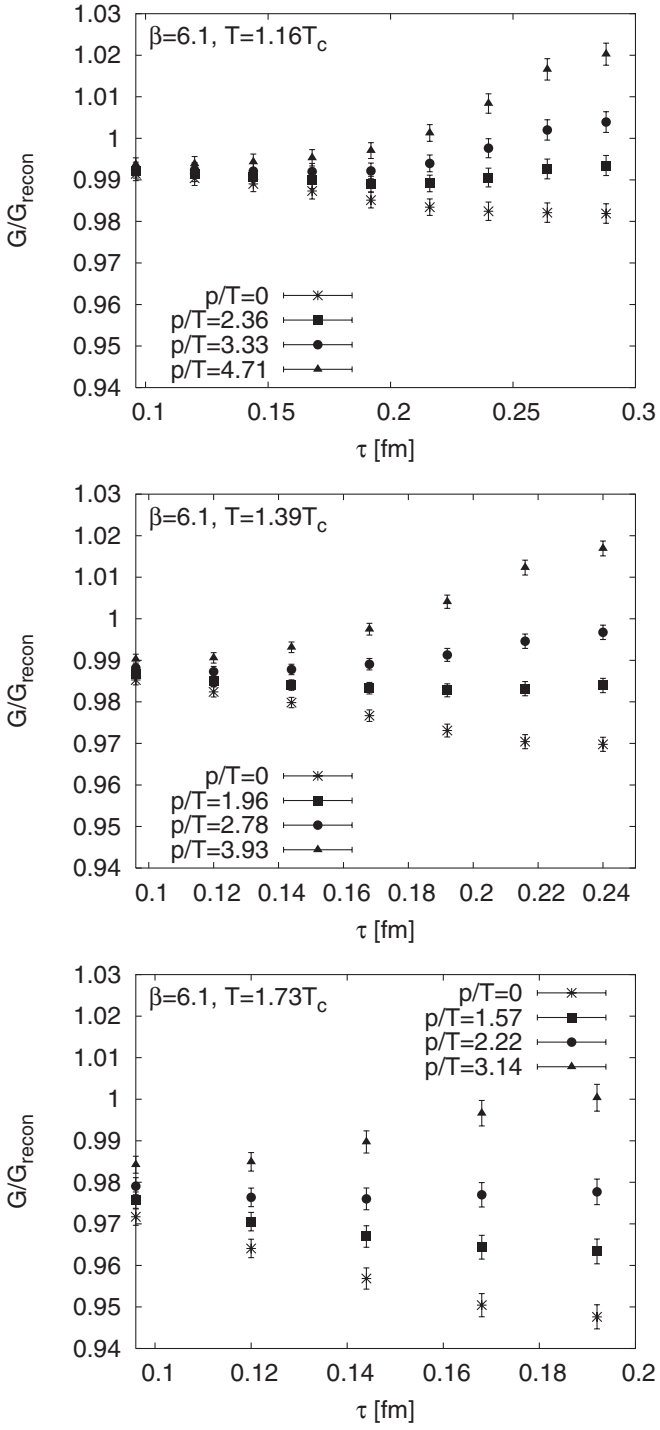

FIG. 20. Pseudoscalar correlators at finite spatial momenta calculated at three different temperatures at $\beta = 6.1$ and $\xi = 4$.

scalar spectral functions for nonzero momenta is significant. This again is in qualitative agreement with the results based on isotropic lattice calculations. It would be interesting to see if the difference in the temperature dependence of the correlators at zero and finite spatial momenta is due to a contribution to the spectral functions below the light cone at finite temperature [24,25].

IX. BOTTOMONIUM SPECTRAL FUNCTIONS AT ZERO TEMPERATURE

The use of Fermilab formulation described in the previous sections allows us to study also bottomonium for the same range of lattice spacings. Usually bottomonium is studied using lattice NRQCD (see e.g. Ref. [55]). So far the only study of bottomonium within the relativistic framework was presented in Ref. [49]. The simulation parameters for bottomonium are summarized in Table IV. As before the lattice spacing is fixed by the Sommer scale r_0, assuming $r_0 = 0.5$ fm. The values of r_0 for $\beta = 5.9$ and 6.1 are taken from Ref. [45], while for $\beta = 6.3$ we use the extrapolation described in Sec. IV. The bare quark mass, the bare velocity of light ν_t as well as the clover coefficients were taken from Ref. [49]. Note that the lattice spacings determined from r_0 are about 20% smaller than in Ref. [49] where it was determined from bottomonium ${}^1P_1 - \overline{1S}$ mass splitting. As the result our estimates of the Υ mass are smaller than those in Ref. [49]. However, if we use the values of the lattice spacing quoted in Ref. [49] to calculate the physical masses we find good agreement.

In our study we will stick to the value of the lattice spacing determined from r_0 as it agrees reasonably well with the lattice spacings extracted from the charmonium ${}^1P_1 - \overline{1S}$ splitting. This splitting is apparently less sensitive to the effect of quenching. The bottomonium ${}^1P_1 - \overline{1S}$ splitting, on the other hand, is more sensitive to quenching errors as well as more difficult to estimate precisely on the lattice. In Table IV we also show the Υ masses.

Using MEM we analyzed the spectral functions in different channels for all three lattice spacings. In Fig. 21 we show the spectral functions in the pseudoscalar channel. Since the physical quark mass is different at different lattice spacings we shifted the horizontal scale by the difference of the calculated Υ-mass and the corresponding

TABLE IV. Simulation parameters for bottomonium at zero temperature

β	5.9	6.1	6.3
$N_s \times N_t$	$8^3 \times 96$	$16^3 \times 96$	$16^3 \times 128$
ξ	3.1390	3.2108	3.2686
r_0/a	3.179(9)	5.189(21)	6.91(2)
a_t^{-1} [GeV]	5.882(25)	8.181(32)	10.89(3)
$C_{\rm sw}^s$	2.0598	1.9463	1.7680
$C_{\rm sw}^t$	1.1277	1.0984	1.0505
m_0	1.120	0.670	0.494
ν_t	1.50	1.573	1.50
$c(0)$	1.026(32)	0.979(7)	1.004(19)
$M_{\Upsilon(1S)}$ [GeV]	8.317(1)	8.084(2)	9.097(1)
L_s [fm]	1.07	1.54	1.16
configs	700	650	650

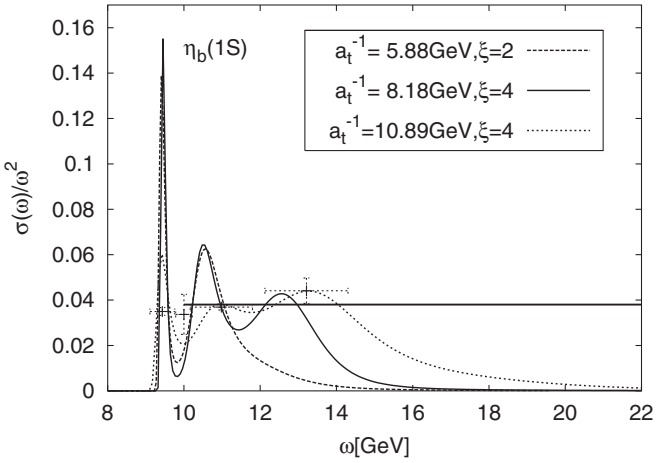

FIG. 21. The pseudoscalar bottomonium spectral function at zero temperature for different lattice spacings.

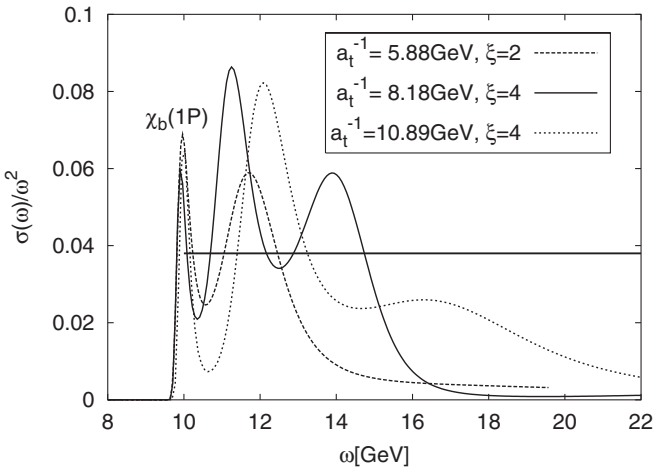

FIG. 22. The scalar bottomonium spectral function at zero temperature for different lattice spacings.

experimental value. We can see that the first peak in the spectral function corresponds to the $\eta_b(1S)$ state and its position is independent of the lattice spacing. The remaining details of the spectral functions are cut-off dependent and we cannot distinguish the excited states from the continuum. The position and the amplitude of the first peak in the spectral functions is in good agreement with the results of simple exponential fit. As in the charmonium case the maximal energy $\omega_{\max}$ for which the spectral function is nonzero scales approximately as a_s^{-1}. Similar results have been obtained in the vector channel.

The spectral function in the scalar channel is shown in Fig. 22. As it was the case for charmonium the correlators in this channel are more noisy than in the pseudoscalar channel and as a result it is more difficult to reconstruct the spectral function. Nevertheless we are able to reconstruct the χ_{b0} state which is the first peak in the spectral function. The peak position and the amplitude are in reasonable agreement with the result of simple exponential fit.

X. BOTTOMONIA AT FINITE TEMPERATURE

Having calculated the bottomonium spectral function at zero temperature we can study the temperature dependence of bottomonium correlators to see medium modification of bottomonia properties. The parameters of the finite temperature simulations are summarized in Table V.

In Fig. 23 we show G/G_{recon} for vector and pseudoscalar channel at different lattice spacings. This ratio appears to be temperature independent and very close to unity up to quite high temperatures. This is consistent with the expectation that $1S$ bottomonia are smaller than $1S$ charmonia and thus less effected by the medium. They could survive till significantly higher temperatures. Compared to charmonium case the difference between the pseudoscalar and vector channels is smaller. This is also expected as the transport contribution which is responsible for this difference is proportional to $\chi_s(T) \sim \exp(-m_{c,b}/T)$, and thus is much smaller for bottom quarks.

The temperature dependence of the scalar correlator is shown in Fig. 24. Contrary to the pseudoscalar and vector correlators it shows strong temperature dependence and G/G_{recon} is significantly larger than unity already at $1.1T_c$. Since the size and the binding energy of $1P$ bottomonium states are comparable to that of the $1S$ charmonium states one would expect a much smaller temperature dependence. The data on the other hand shows temperature dependence which is even larger than for $1P$ charmonium states. This may suggest that the $1P$ bottomonium states are strongly modified or maybe even dissolved at $T \simeq 1.1 - 1.2T_c$. Further investigation are needed to clarify what happens to $1P$ bottomonium states above the deconfinement tran-

TABLE V. Simulation parameters for bottomonium at finite temperature. We assumed $r_0 T_c = 0.7498(50)$ corresponding to $T_c = 295(2)$ MeV.

$\beta = 5.9$			$\beta = 6.1$			$\beta = 6.3$		
lattice	T/T_c	#config	lattice	T/T_c	#config	lattice	T/T_c	#config
$8^3 \times 16$	1.25	700	$16^3 \times 24$	1.16	500	$16^3 \times 32$	1.15	440
$8^3 \times 12$	1.66	700	$16^3 \times 20$	1.39	500	$16^3 \times 24$	1.54	100
$8^3 \times 8$	1.66	1000	$16^3 \times 16$	1.73	500	$16^3 \times 20$	1.85	100
$8^3 \times 6$	3.32	1000				$16^3 \times 16$	2.31	100

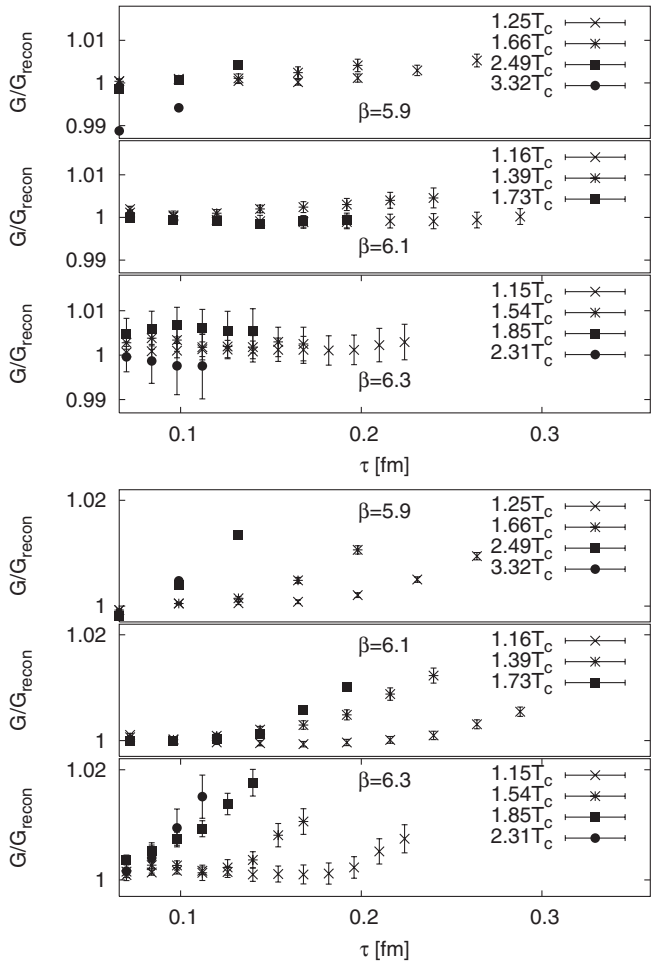

FIG. 23. The ratio G/G_{rec} in the pseudoscalar (top) and vector (bottom) channels at different lattice spacings.

sition. Model studies of the P-wave bottomonium correlators suggest that its large change may be due to the modification of the continuum part of the spectral functions and

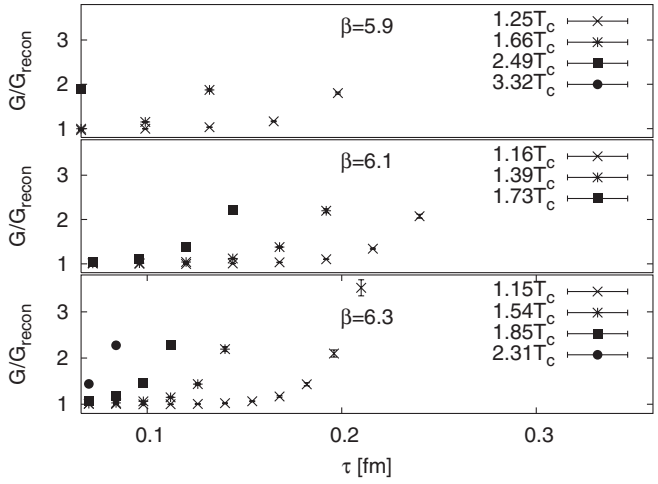

FIG. 24. The ratio G/G_{rec} in the scalar channel for different lattice spacings.

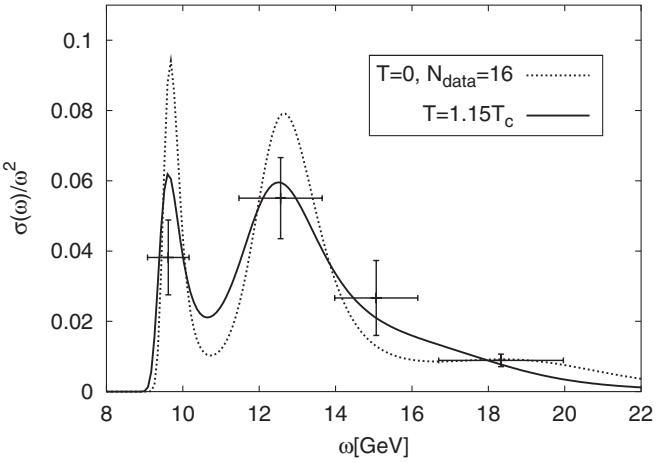

FIG. 25. The pseudoscalar bottomonium spectral function at finite temperature.

not to the dissolution or strong modification of the ground state [11].

We have tried to reconstruct the spectral functions at finite temperature for $\beta = 6.3$. For the pseudoscalar channel the results are shown in Fig. 25. As in the charmonium case we compare the finite temperature spectral function with the zero temperature spectral function obtained with the same number of data points and time interval. As expected the spectral function shows no temperature dependence within errors. On the other hand we could not reliably reconstruct the scalar spectral function at finite temperature, the probability $P[\alpha|Dm]$ showed no maximum as the function of α. Presumably much more statistics is needed to get some information about the scalar spectral function.

XI. CONCLUSIONS

In this paper we investigated quarkonium correlators at zero and finite temperature in quenched QCD using anisotropic lattices and the Fermilab formalism for the heavy quarks. In our investigations we used a variety of different lattice spacings to control cut-off effects in the quarkonium correlators and spectral functions. Using the Maximum Entropy Method we have calculated the spectral functions both at zero and finite temperatures. This was done using a newly developed algorithm for the MEM analysis which does not rely on singular value decomposition. It appeared to be more stable than the Bryan algorithm used so far in the analysis of the meson spectral functions. Therefore we could for the first time reliably calculate the charmonium spectral functions at zero temperature identifying the main structures: ground state, excited states and the continuum. Using the zero temperature results as the base line we investigated the temperature dependence of charmonium correlators at finite temperature at different lattice spacings and showed that it is qualitatively the same for all lattice spacings. We studied the charmonium spectral functions at

finite temperature paying attention to systematic effects arising from the fact that the time interval at finite temperature as well as the number of data points decreases with increasing temperature. We found that the spectral functions in the pseudoscalar channel do not change up to temperatures $1.5T_c$ within systematic and statistical errors of our calculations. We have also learned that it is difficult to make statements about the survival of charmonium states based solely on the shape of the spectral function as it is distorted by the limited time extent and strongly depends on the default model. On the other hand the small temperature dependence of the pseudoscalar spectral function up to $1.5T_c$ holds for all default models. The correlation functions in all channels corresponding to $1P$ states show very different behavior. Together with the results for the scalar spectral functions this suggests the melting of the $1P$ charmonium states at temperature $T = 1.1 - 1.2T_c$. In general, most of our findings in charmonium sector is in reasonable agreement with results known from studies on fine isotropic lattices [17]. We also identify the transport contribution in the vector correlators for the first time.

Our investigations in the bottomonium sector are less detailed. We were able to reconstruct the bottomonium spectral functions at zero temperature and show that the first peak is not affected by lattice artifacts. Nonetheless the spectral functions are less accurate than for charmonium. We were not able to reconstruct reliably the bottomonium spectral functions at finite temperature. The reason is that because of the large quark mass the correlators decay fast and the signal is poor. The temperature dependence of the correlators suggests that the $1S$ bottomonium state can survive till much higher temperature than the charmonium states. On the other hand we see, unexpectedly, drastic changes in the $1P$ bottomonium correlators right after deconfinement transition. To clarify the fate of the $1P$ bottomonium states further studies are clearly needed. They presumably should rely on NRQCD where the large bottom quark mass is integrated out.

The use of anisotropic lattices and Fermilab approach reduces discretization effects and allows to study the problem of quarkonium dissolution on coarser lattices. In fact the analysis of the temperature dependence of the correlation functions shows that they can be reliably studied already for lattice spacings $a_s^{-1} = 2.0$ GeV. Although the temperature dependence of the correlators turns out to be the same for all lattice spacings studied in this paper, we clearly see quantitative differences. This is important when we want to extend the studies of quarkonium spectral functions to full QCD, where the lattice spacing is main limiting factor. Preliminary results from calculations of charmonium spectral functions in full QCD have been reported in Ref. [56]. These results are in qualitative agreement with findings in quenched QCD. However, no quantitative analysis has been performed so far to estimate the effect of sea quarks. To get sufficiently close to the continuum limit in the analysis of the correlation function the spatial lattice spacing should presumably be smaller than $(4\ \text{GeV})^{-1}$, i.e. it should be in the range used in studies with isotropic lattices [17].

ACKNOWLEDGMENTS

This work has been supported by U.S. Department of Energy under Contract No. DE-AC02-98CH10886 and by SciDAC project. A. V. was partially supported by NSF-PHY-0309362. K. P. is supported by Marie Curie Excellence Grant under contract No. MEXT-CT-2004-013510. A. J. is supported by Hungarian Science Fund OTKA (F043465). Support through LDRD funds at Brookhaven National Laboratory is also greatly appreciated. Most of numerical calculations have been done on QCDOC supercomputer at RIKEN-BNL Research Center. Authors used Columbia Physics System (CPS) with high-performance clover inverter by P. Boyle and other parts by RBC collaboration. Special thanks to C. Jung for his generous help with CPS. We would like to thank F. Karsch and Á. Mócsy for careful reading of the manuscript and valuable comments. The final analysis of the lattice data has been done during the stay of one of the authors (P. P.) at the Institute for Nuclear Theory (INT) at Washington University. We are grateful to INT for their support.

APPENDIX

In this appendix we present some technical details on the calculations of the quarkonium spectral functions. To study the reliability of MEM at zero temperature we compare the

TABLE VI. The zero temperature charmonium masses and amplitudes obtained from MEM and compared to 2-exponential fit with jackknife errors. We show the systematic errors of the fit procedure in the square brackets.

	$\beta = 5.7,\ \xi = 2$		$\beta = 5.9,\ \xi = 2$		$\beta = 6.1,\ \xi = 2$		$\beta = 6.1,\ \xi = 4$		$\beta = 6.5,\ \xi = 4$	
	MEM	2-exp	MEM	2-exp	MEM	2-exp	MEM	2-exp	MEM	2-exp
$A_{sc}(n=1)$	0.41(2)	0.42(3)	0.211(19)	0.215(8)[9]	0.136(10)	0.111(7)[4]	0.037(6)	0.056(6)[1]	0.028(4)	0.021(1)[8]
$m_{sc}(n=1)$	1.832(8)	1.85(1)	1.224(45)	1.218(8)[2]	0.842(6)	0.840(4)[1]	0.410(3)	0.420(3)[4]	0.255(5)	0.251(1)[5]
$A_{ps}(n=1)$	1.83(2)	1.81(1)[2]	0.711(10)	0.714(2)[6]	0.32(11)	0.327(5)[2]	0.195(6)	0.1760(1)[102]	0.042(2)	0.0423(5)
$m_{ps}(n=1)$	1.5859(0)	1.5870(4)[3]	1.0472(0)	1.0482(1)[2]	0.727(7)	0.7285(4)[2]	0.363(5)	0.3630(3)[11]	0.2147(0)	0.2154(2)
$A_{ps}(n=2)$	5.22(7)	4.07(7)[88]	1.33(13)	1.8(1)[5]	0.72(31)	0.93(5)[14]	0.61(5)	0.69(36)[21]	0.107(13)	0.117(7)
$m_{ps}(n=2)$	2.15(4)	2.018(5)[44]	1.30(2)	1.34(1)[3]	1.01(8)	0.967(9)[14]	0.50(2)	0.481(15)[6]	0.281(8)	0.285(2)

TABLE VII. The *ad hoc* renormalization constants for charmonium used in Figs. 2, 3, 5–7, and 15–19 in different channels.

β, ξ	6.1, 2	6.1, 4	6.5, 4
Z_{PS}	0.374	0.447	0.447
Z_{VC}	0.343	0.447	0.426
Z_{SC}	0.534	0.791	0.620
Z_{AX}	0.592	0.949	0.707

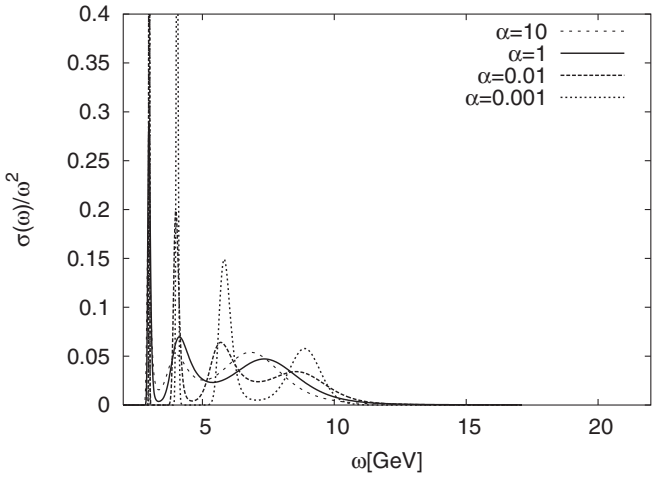

FIG. 26. The pseudoscalar spectral function for different values of α. The spectral functions were calculated on $16^3 \times 96$ lattice at $\beta = 6.1$, $\xi = 4$.

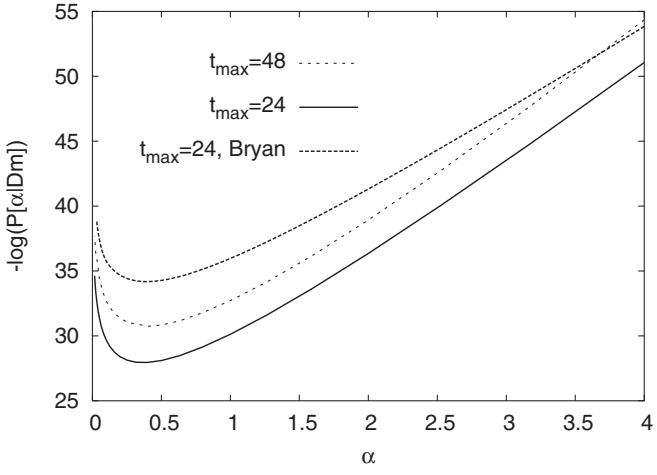

FIG. 27. The conditional probability $P[\alpha|Dm]$ for different algorithms and different $t_{\max}$ corresponding to the pseudoscalar spectral function calculated on $16^3 \times 96$ lattice at $\beta = 6.1$, $\xi = 4$.

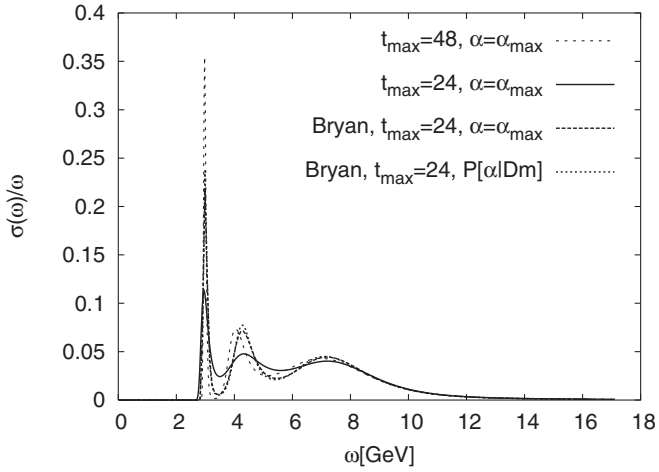

FIG. 28. The pseudoscalar spectral function calculated on $16^3 \times 96$ lattice at $\beta = 6.1$, $\xi = 4$ using the algorithm described in this paper and the Bryan algorithm for $\alpha = \alpha_{\max}$. Also shown in the figure is the spectral function obtained by integrating over α with the weight $P[\alpha|Dm]$. See the main text for further details.

masses and amplitudes of different states obtained from MEM and simple 2-exponential fit. This comparison is shown in Table VI. We also tried to estimate the systematic errors in the fit by allowing higher excited states (3 exponential fit). We show this systematic uncertainty in the square brackets. One can see that we have a good agreement for the ground state in pseudoscalar channel (η_c), the small disagreement in the values of the meson masses (typically appearing in the 4th digit) is the consequence of the discretization in ω. We have checked that for sufficiently fine binning of the spectral function this remaining error could be removed. For the scalar channel we find agreement between the results of the fit and MEM within estimated errors, with the only exception being $\beta = 6.1$

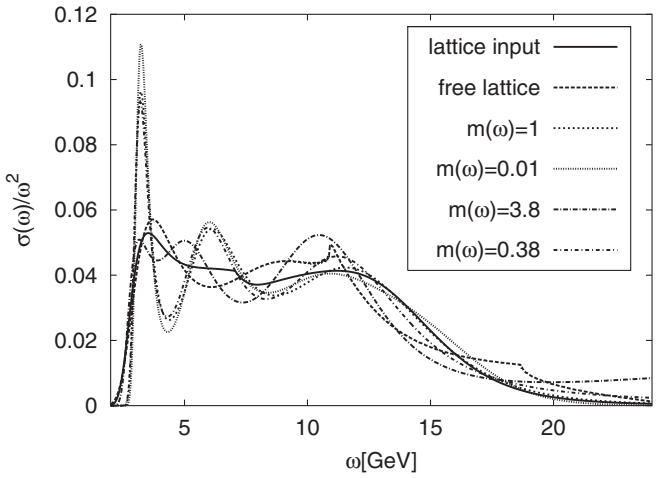

FIG. 29. The default model dependence of the pseudoscalar spectral function at $1.2T_c$ calculated on $24^3 \times 40$ lattice with $\beta = 6.5$.

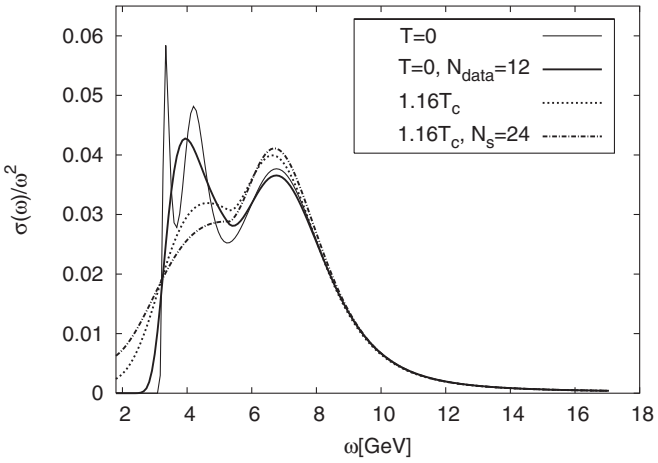

FIG. 30. The scalar spectral function at $1.16T_c$ and at zero temperature reconstructed using $\tau_{\max} = 12$ calculated with the default model coming from the high energy part of the zero temperature spectral function (see text). Also shown the zero temperature spectral function calculated using all data points and $m(\omega) = 1$.

where we find small deviation for the amplitudes which are outside the errors. In the pseudoscalar channel we find also an agreement for the masses and amplitudes of the excited states within the estimated errors.

To compare the spectral functions at different lattice spacings one needs the renormalization constants of different quark bilinears. For the lattice fermions used in the present paper these have not been calculated. Therefore we introduced *ad hoc* renormalization constants which are shown in Table VII.

The real parameter α enters into MEM through Eq. (12). Therefore we have studied the dependence of the spectral functions on α. For the pseudoscalar channel at zero temperature this is shown in Fig. 26. To get rid of the alpha dependence of the spectral function one calculates the conditional probability $P[\alpha|DH]$. For sufficiently good quality Monte Carlo data this function has a unique maximum at some alpha. This is shown in Fig. 27 for the new algorithm used in this paper as well as for the Bryan algorithm. The spectral functions calculated with the new algorithm and the Bryan algorithm are shown in Fig. 28.

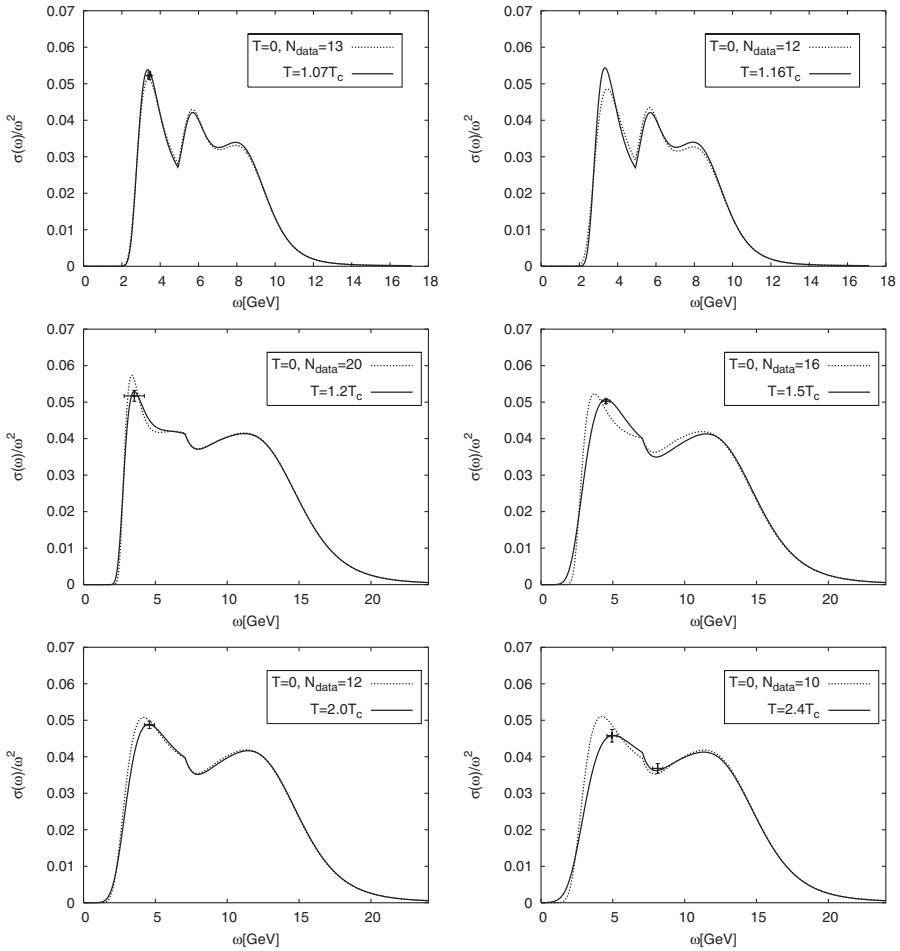

FIG. 31. The pseudoscalar spectral function at different temperatures together with the zero temperature spectral functions reconstructed using default model coming from the high energy part of the zero temperature spectral function (see text).

At finite temperature the dependence of the spectral functions on the default model becomes important. Therefore we investigated the default model dependence of the spectral function. First we used different functional forms for the default model, $m(\omega) \sim \omega^2$ motivated by the free spectral functions of the continuum QCD and $m(\omega) =$ const. We also considered the free lattice spectral function calculated in Ref. [24] as a default model. In Fig. 29 we show the pseudoscalar spectral function at $1.2T_c$ calculated with different default models. The figures shows that the default model dependence of the spectral function is significant, in particular, the first peak is not present for all default models. Following Ref. [17] we have used the high energy part of the zero temperature lattice spectral function and matched it to the ω^2 behavior at some energy ω_{th} above the energy region where no individual resonances can be seen. In the pseudoscalar channel at $\beta = 6.5$ we have chosen $\omega_{\text{th}} \simeq 7$ GeV, for $\beta = 6.1$ we have chosen $\omega_{\text{th}} \simeq 5$ GeV in the pseudoscalar channel and $\omega_{\text{th}} \simeq 5.5$ GeV in the scalar channel. In Fig. 30 we show the scalar spectral function at zero temperature with $N_{\text{data}} = 12$ and at $T = 1.16T_c$ for this type of the default model. The scalar spectral function shows significant change with the temperature in this case too. We analyzed the pseudoscalar spectral function with this type of the default model and the result of this analysis is shown in Fig. 31. For this choice of the default model significant temperature dependence can be seen only for $T = 2.4T_c$. In the figure we also show the errors where appropriate. We find that the statistical errors are much smaller for this default model.

[1] T. Matsui and H. Satz, Phys. Lett. B **178**, 416 (1986).
[2] F. Karsch, M. T. Mehr, and H. Satz, Z. Phys. C **37**, 617 (1988).
[3] G. Röpke, D. Blaschke, and H. Schulz, Phys. Rev. D **38**, 3589 (1988).
[4] T. Hashimoto *et al.*, Z. Phys. C **38**, 251 (1988).
[5] S. Digal, P. Petreczky, and H. Satz, Phys. Lett. B **514**, 57 (2001).
[6] S. Digal, P. Petreczky, and H. Satz, Phys. Rev. D **64**, 094015 (2001).
[7] E. V. Shuryak and I. Zahed, Phys. Rev. D **70**, 054507 (2004).
[8] C. Y. Wong, Phys. Rev. C **72**, 034906 (2005).
[9] C. Y. Wong and H. W. Crater, hep-ph/0610440.
[10] A. Mócsy and P. Petreczky, Eur. Phys. J. C **43**, 77 (2005).
[11] A. Mócsy and P. Petreczky, Phys. Rev. D **73**, 074007 (2006).
[12] A. Mócsy, P. Petreczky, and J. Casalderrey-Solana, hep-ph/0609205; A. Mocsy and P. Petreczky, J. Phys. G **32**, S515 (2006).
[13] W. M. Alberico, A. Beraudo, A. De Pace, and A. Molinari, Phys. Rev. D **72**, 114011 (2005).
[14] D. Cabrera and R. Rapp, hep-ph/0610254.
[15] T. Umeda, K. Nomura, and H. Matsufuru, Eur. Phys. J. C **39S1**, 9 (2005).
[16] M. Asakawa and T. Hatsuda, Phys. Rev. Lett. **92**, 012001 (2004).
[17] S. Datta, F. Karsch, P. Petreczky, and I. Wetzorke, Phys. Rev. D **69**, 094507 (2004).
[18] K. Petrov, A. Jakovác, P. Petreczky, and A. Velytsky, PoS, LAT2005 (2005) 153 [hep-lat/0509138].
[19] P. Petreczky, K. Petrov, D. Teaney, and A. Velytsky, PoS, LAT2005 (2005) 185 [hep-lat/0510021].
[20] A. Jakovác, P. Petreczky, K. Petrov, and A. Velytsky, hep-lat/0603005.
[21] A. Velytsky, hep-lat/0609013.
[22] M. Le Bellac, *Thermal Field Theory* (Cambridge University Press, Cambridge, England, 1996).
[23] E. Braaten, R. D. Pisarski, and T. C. Yuan, Phys. Rev. Lett. **64**, 2242 (1990).
[24] F. Karsch, E. Laermann, P. Petreczky, and S. Stickan, Phys. Rev. D **68**, 014504 (2003).
[25] G. Aarts and J. M. Martinez Resco, Nucl. Phys. **B726**, 93 (2005).
[26] M. Asakawa, T. Hatsuda, and Y. Nakahara, Prog. Part. Nucl. Phys. **46**, 459 (2001).
[27] G. P. Lepage, B. Clark, C. T. H. Davies, K. Hornbostel, P. B. Mackenzie, C. Morningstar, and H. Trottier, Nucl. Phys. B, Proc. Suppl. **106**, 12 (2002).
[28] R. K. Bryan, Eur. Biophys J. **18**, 165 (1990).
[29] Y. Nakahara, M. Asakawa, and T. Hatsuda, Phys. Rev. D **60**, 091503 (1999).
[30] T. Yamazaki *et al.* (CP-PACS Collaboration), Phys. Rev. D **65**, 014501 (2001).
[31] F. Karsch, E. Laermann, P. Petreczky, S. Stickan, and I. Wetzorke, Phys. Lett. B **530**, 147 (2002).
[32] F. Karsch, S. Datta, E. Laermann, P. Petreczky, S. Stickan, and I. Wetzorke, Nucl. Phys. **A715**, 701 (2003).
[33] S. Datta, F. Karsch, P. Petreczky, and I. Wetzorke, Nucl. Phys. B, Proc. Suppl. **119**, 487 (2003).
[34] M. Asakawa, T. Hatsuda, and Y. Nakahara, Nucl. Phys. **A715**, 863 (2003); Nucl. Phys. B, Proc. Suppl. **119**, 481 (2003).
[35] T. Blum and P. Petreczky, Nucl. Phys. B, Proc. Suppl. **140**, 553 (2005).
[36] P. Petreczky, J. Phys. G **30**, S431 (2004).
[37] P. Petreczky, F. Karsch, E. Laermann, S. Stickan, and I. Wetzorke, Nucl. Phys. B, Proc. Suppl. **106**, 513 (2002).
[38] C. R. Allton, J. E. Clowser, S. J. Hands, J. B. Kogut, and C. G. Strouthos, Phys. Rev. D **66**, 094511 (2002).
[39] K. Langfeld, H. Reinhardt, and J. Gattnar, Nucl. Phys. **B621**, 131 (2002).
[40] H. R. Fiebig, Phys. Rev. D **65**, 094512 (2002).
[41] K. Sasaki, S. Sasaki, and T. Hatsuda, Phys. Lett. B **623**, 208 (2005).
[42] P. Chen, Phys. Rev. D **64**, 034509 (2001).

[43] T. R. Klassen, Nucl. Phys. **B533**, 557 (1998).
[44] R. Sommer, Nucl. Phys. **B411**, 839 (1994).
[45] R. G. Edwards, U. M. Heller, and T. R. Klassen (unpublished).
[46] C. R. Allton, Nucl. Phys. B, Proc. Suppl. **53**, 867 (1997); hep-lat/9610016.
[47] M. Okamoto *et al.* (CP-PACS Collaboration), Phys. Rev. D **65**, 094508 (2002).
[48] A. Gray *et al.*, Phys. Rev. D **72**, 094507 (2005).
[49] X. Liao and T. Manke, Phys. Rev. D **65**, 074508 (2002).
[50] M. Jarrell and J. M. Gubernatis, Phys. Rep. **269**, 133 (1996).
[51] S. Necco, Nucl. Phys. **B683**, 137 (2004).
[52] P. Petreczky and D. Teaney, Phys. Rev. D **73**, 014508 (2006).
[53] H. Iida, T. Doi, N. Ishii, H. Suganuma, and K. Tsumura, Phys. Rev. D **74**, 074502 (2006).
[54] S. Datta, F. Karsch, S. Wissel, P. Petreczky, and I. Wetzorke, hep-lat/0409147.
[55] C. T. Davies *et al.*, Phys. Rev. D **50**, 6963 (1994).
[56] G. Aarts, C. R. Allton, R. Morrin, A. P. O. Cais, M. B. Oktay, M. J. Peardon, and J. I. Skullerud, hep-lat/0610065.